Nonlinear Control of Particulate Processes

Timothy Chiu and Panagiotis D. Christofides
Dept. of Chemical Engineering, University of California, Los Angeles, CA 90095

A general methodology is proposed for the synthesis of practically-implementable nonlinear output feedback controllers for spatially-homogeneous particulate processes modeled by population balance equations. Initially, a nonlinear model reduction procedure based on a combination of the method of weighted residuals and the concept of approximate inertial manifold is presented for the construction of low-order ordinary differential equation (ODE) systems that accurately reproduce the dominant dynamics of the particulate process. These ODE systems are then used for the synthesis of nonlinear low-order output feedback controllers that enforce exponential stability in the closed-loop system and achieve particle-size distributions with desired characteristics. Precise closed-loop stability conditions are given and controller implementation issues are discussed. The proposed nonlinear control method is successfully applied to a continuous crystallizer, and is shown to outperform a proportional-integral controller and cope effectively with model uncertainty and measurement delays.

Introduction

Particulate processes (also known as dispersed-phase processes) are characterized by material domains that are comprised of a continuous phase and a dispersed phase and are essential in making many high-value industrial products. Examples include the crystallization of proteins for pharmaceutical applications, the emulsion polymerization reactors for the production of latex, and the titania powder aerosol reactors used in the production of white pigments. It is now well understood that the physicochemical and mechanical properties of materials made with particulates depend heavily on the characteristics of the corresponding particle-size distribution (PSD) (for example, a nearly monodisperse PSD is required for titania pigments to obtain the maximum hiding powder per unit mass). Therefore, the problem of synthesizing and implementing high-performance model-based feedback control systems on particulate processes to achieve PSDs with desired characteristics has significant industrial value. On the other hand, recent developments in measurement technology allow the accurate and fast on-line measurement of key process variables, including PSDs [see Rawlings et al. (1993) for an excellent review of the available measurement technology], which can then be used for feedback control purposes.

Population balances have provided a natural framework for the mathematical modeling of PSDs (see, for example, the tutorial article by Hulburt and Katz (1964) and the review article by Ramkrishna (1985)), and have been successfully used to describe PSDs in emulsion polymerization reactors (Dimitratos et al., 1994), crystallizers (Rawlings et al., 1993), and aerosol reactors (Friedlander, 1977; Williams and Loyalka, 1991). Application of population balances to particulate processes typically leads to systems of nonlinear partial integro-differential equations that describe the rate of change of the PSD. The population balances are coupled with the material and energy balances that describe the rate of change of the state variables of the continuous phase (these are usually systems of nonlinear differential equations, which include integrals over the entire particle-size spectrum), leading to complete particulate process models.

The nonlinear (owing to complex growth, nucleation, agglomeration and breakage mechanisms, and their Arrhenius dependence on temperature) and distributed nature of population balances has motivated extensive research on the development of efficient numerical methods for the accurate computation of their solution. Examples of solution methods for continuous population balances include the method of self-preserving distributions (Friedlander, 1977), the method of weighted residuals (Ramkrishna, 1985; Gelbard and Seinfeld, 1978), the sectional method (Gelbard et al., 1980; Langrebe and Pratsinis, 1990), and discretization via fixed/moving pivot techniques (Kumar and Ramkrishna, 1996a,b), while methods for the solution of discretized population balances

Correspondence concerning this article should be addressed to P. D. Christofides.

have been proposed in Hounslow (1990), and Hill and Ng (1996). An excellent review of results in this area can be found in Ramkrishna (1985). The ability to accurately solve population balance models motivated numerous research studies on the dynamics of particulate processes. These studies confirmed the existence of a wide range of complex static and dynamic phenomena including multiple steady states and sustained oscillations [see, for example, Lei et al. (1971), Jerauld et al. (1983), and Rawlings and Ray (1987a,b) for a theoretical analysis of oscillatory behavior in crystallizers and emulsion polymerization reactors, respectively], which had been previously observed in experimental studies [see the classic book by Randolph and Larson (1988) for results and references]. The highly nonlinear and oscillatory behavior of many particulate processes implies the need to implement nonlinear model-based feedback controllers in order to ensure a stable and efficient operation.

In spite of the rich literature on population balance modeling, numerical solution, and dynamical analysis of particulate processes, research on model-based control of such processes has been very limited. Specifically, previous efforts have mainly focused on the understanding of fundamental control-theoretic properties (controllability and observability) of population balance models (Semino and Ray, 1995a) and the application of conventional control schemes (such as proportional-integral and proportional-integral-derivative control, self-tuning control) to crystallizers and emulsion polymerization processes [see, for example, Semino and Ray (1995b); Rohani and Bourne (1990); Dimitratos et al. (1994) and the references therein]. Notable exceptions on model-based control of particulate processes include an optimization-based control method which was developed in Eaton and Rawlings (1990) and successfully applied to a batch crystalization process, as well as nonlinear state feedback control of a cell culture in Kurtz et al. (1998). The main difficulty in synthesizing nonlinear model-based feedback controllers for particulate processes is the distributed parameter nature of the population balance models which does not allow their direct use for the synthesis of low-order (and therefore, practically-implementable) output feedback controllers. Furthermore, a direct application of the aforementioned solution methods to derive finite-dimensional approximations of the population balance models may lead to ODE systems of very high order, which are inappropriate for the synthesis of low-order controllers.

This article focuses on nonlinear feedback control of spatially-homogeneous particulate processes modeled by a class of nonlinear partial integro-differential equation systems. The objective is to develop a general and rigorous method for the synthesis of practically-implementable nonlinear model-based feedback controllers that enforce the desired stability and performance specifications (such as PSDs with desired total mass and mean particle size) in the closed-loop system.

A general class of nonlinear partial integro-differential equation systems is initially given, which describes the majority of spatially-homogeneous particulate processes, and a crystallizer example is used to motivate the proposed approach for control of particulate processes. Then, a model reduction procedure based on a combination of the method of weighted residuals and the concept of approximate inertial manifold is proposed for the construction of low-order ODE systems that accurately reproduce the dominant dynamics of the particulate process. These ODE systems are subsequently used for the synthesis of nonlinear low-order output feedback controllers that enforce exponential stability in the closed-loop system and achieve a desired PSD. Precise closed-loop stability conditions are given and controller implementation issues are addressed. The performance and robustness of the proposed control method are successfully tested through simulations on a continuous crystallizer and are shown to be superior to the ones of a proportional-integral control scheme.

Modeling and Dynamics of Particulate Processes

Particulate process model

We focus on spatially homogeneous particulate processes with simultaneous particle growth, nucleation, agglomeration, and breakage and consider the case of a single internal particle coordinate which, for the sake of exposition, is assumed to be the particle size. Applying a dynamic material balance on the number of particles of size r to $r + dr$ (population balance), we obtain the following general nonlinear partial integro-differential equation which describes the rate of change of the PSD $n(r, t)$

$$\frac{\partial n}{\partial t} = -\frac{\partial [G(x,r)n]}{\partial r} + w(n, x, r) \tag{1}$$

where $n(r, t) \in L_2[0, r_{\max})$ ($L_2[0, r_{\max})$ is the Hilbert space of continuous functions defined on the interval $[0, r_{\max})$), $r \in [0, r_{\max}]$ is the particle size, and $r_{\max}$ is the maximum particle size (which may be infinity), t is the time and $x \in \mathbb{R}^n$ is the vector of state variables which describe properties of the continuous phase (such as solute concentration, temperature and pH in a crystallizer). See Eq. 2 below for the system that describes the dynamics of x. $G(x, r)$ and $w(n, x, r)$ are nonlinear scalar functions whose physical meaning can be explained as follows: $G(x, r)$ accounts for particle growth through condensation and is usually referred to as growth rate. It usually depends on the concentrations of the various species present in the continuous phase, the temperature of the process, and the particle size. On the other hand, $w(n, x, r)$ represents the net rate of introduction of new particles into the system. It includes all the means by which particles appear or disappear within the system including particle agglomeration (merging of two particles into one), breakage (division of one particle to two), as well as, nucleation of particles of size $r \geq 0$ and particle feed and removal.

The rate of change of the continuous-phase variables x can be derived by a direct application of mass and energy balances to the continuous phase and is given by a nonlinear integro-differential equation system of the general form

$$\dot{x} = f(x) + g(x)u(t) + A\int_0^{r_{\max}} a(n, r, x)\,dr \tag{2}$$

where $f(x)$, $a(n, r, x)$ are nonlinear vector functions, $g(x)$ is a nonlinear matrix function, A is a constant matrix, and $u(t) = [u_1\ u_2\ \cdots\ u_m] \in \mathbb{R}^m$ is the vector of manipulated inputs. The term $A\int_0^{r_{\max}} a(n, r, x)dr$ accounts for mass and heat

transfer from the continuous phase to all the particles in the population.

We define a vector of controlled outputs to express the various control objectives (such as regulation of total number of particles, mean particle size, temperature, pH, and so on) as

$$y_i(t) = h_i\left[\int_0^{r_{\max}} c_\kappa(r)\, n(r,t)\, dr,\, x\right], \quad i = 1, \ldots, m,\ \kappa = 1, \ldots, l \tag{3}$$

where $y_i(t)$ is the ith controlled output, $h_i[\int_0^{r_{\max}} c_\kappa(r) n(r,t) dr, x]$ is a nonlinear smooth scalar function of its arguments, and $c_\kappa(r)$ is a known smooth function of r which depends on the desired performance specifications. To simplify the notation of the theoretical development of this article, we will not consider measured outputs separately from controlled outputs, which means that we need to assume the availability of on-line measurements of the controlled outputs $y_i(t)$.

Throughout this article we will use the inner product and norm in $L_2[0, r_{\max})$, which are defined, respectively, as

$$(\phi_1, \phi_2) = \int_0^{r_{\max}} \phi_1(z)\, \phi_2(z)\, dz, \quad \|\phi_1\|_2 = (\phi_1, \phi_1)^{1/2} \tag{4}$$

where ϕ_1, ϕ_2 are two elements of $L_2[0, r_{\max})$. Furthermore, the order of magnitude and Lie derivative notations will be needed in our development. In particular, $\delta(\epsilon) = O(\epsilon)$ if there exist positive real numbers k_1 and k_2 such that $|\delta(\epsilon)| \le k_1|\epsilon|$, $\forall |\epsilon| < k_2$, and $L_f \bar{h}$ denotes the standard Lie derivative of a scalar function $\bar{h}(x)$ with respect to the vector function $f(x)$, $L_f^k \bar{h}$ denotes the kth order Lie derivative and $L_g L_f^{k-1} \bar{h}$ denotes the mixed Lie derivative where $g(x)$ is a vector function.

Remark 1. Referring to the general mathematical model of Eqs. 1–2, the following remarks are in order: (a) the particle-size distribution (PSD) function $n(r, t)$ is assumed to be a sufficiently smooth function of its arguments [that is, $n(r, t)$ and its partial derivatives with respect to r and t, up to a desired order, are continuous functions]; this is a reasonable assumption for large-size distributions, even though particles are discrete and their number is integer-valued; (b) a single internal coordinate (particle size) is considered; this is motivated by the majority of industrial particulate process control problems where the central objective is to produce particulates with a desired PSD; (c) the particles are assumed to be small enough so that the environment in which they are dispersed can be adequately described by a local value of its state vector; (d) the vector of manipulated inputs $u(t)$ is a lumped variable (that is, it only depends on time, for example, the inlet concentration of solute in a crystallizer) and the controlled outputs $y_i(t)$ are taken to be nonlinear functions of x and appropriate weighted averages of n (examples of controlled outputs included in this formulation are total mass of particles, mean particle size, solute concentration, process temperature, and pH). Both choices are typical in most practical applications as illustrated by the crystallization process studied in the section Application to a Continuous Crystallizer.

Remark 2. The nonlinear model reduction and controller synthesis results that will be presented in this article can be generalized to particulate processes, which include manipulated inputs in the population balance (such as manipulation of fines destruction rate. See Lei et al. (1971), Randolph et al. (1987), and Remark 6 below) with the following state-space description

$$\begin{aligned}
\frac{\partial n}{\partial t} &= -\frac{\partial[G(x,r)n]}{\partial r} + w(n,x,r) + g_1(n,x,r)u(t) \\
\dot{x} &= f(x) + g_2\left[x, \int_0^{r_{\max}} a_1(n,r,x)\, dr\right] u(t) \\
&\quad + g_3\left[x, \int_0^{r_{\max}} a_2(n,r,x)\, dr\right] \\
y_i(t) &= h_i\left[\int_0^{r_{\max}} c_\kappa(r)\, n(r,t)\, dr, x\right], \\
&\quad i = 1, \ldots, m,\ \kappa = 1, \ldots, l
\end{aligned} \tag{5}$$

where $g_1(n, x, r)$, $g_3[x, \int_0^{r_{\max}} a_2(n, r, x) dr]$, $a_1(n, r, x)$, $a_2(n, r, x)$ are nonlinear vector functions and $g_2[x, \int_0^{r_{\max}} a_1(n, r, x) dr]$ is a nonlinear matrix function.

Dynamics of particulate processes: continuous crystallizer

Crystallization is a particulate process which is widely used in industry for the production of many products including fertilizers, proteins, and pesticides. The fact that the shape of the crystal-size distribution influences significantly the necessary liquid-solid separation, as well as the properties of the product, implies that crystallization requires a population balance in order to be accurately described, analyzed, and controlled. Crystallizers typically exhibit highly oscillatory behavior which suggests the use of feedback control to ensure stable operation and attain a crystal-size distribution with desired characteristics.

We consider a continuous crystallizer (Figure 1), which exhibits highly oscillatory behavior and we show that its domi-

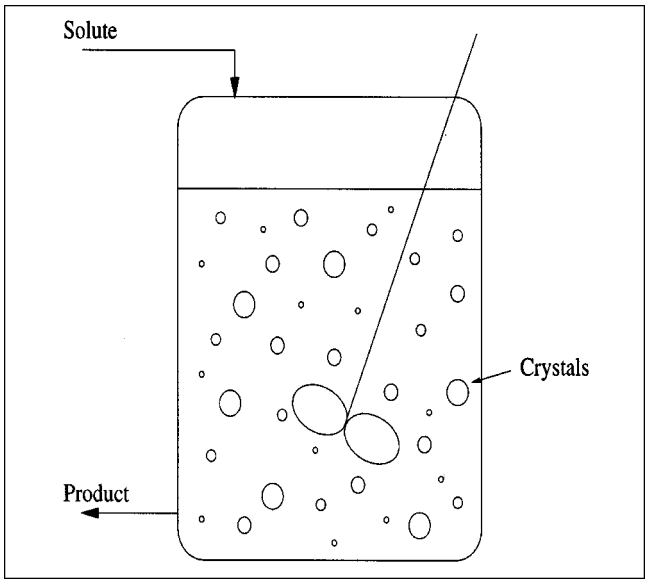

Figure 1. Continuous crystallizer.

nant dynamics can be accurately described by a small set of ODEs; this finding implies that the dominant dynamics of the process are characterized by a small number of degrees of freedom (low-dimensional) and motivate the proposed approach for nonlinear model-based feedback control of particulate processes. Under the assumptions of isothermal operation, constant volume, mixed suspension, nucleation of crystals of infinitesimal size, mixed product removal, a dynamic model for the crystallizer can be derived from a population balance for the particle phase and a mass balance for the solute concentration, and it is of the form (Lei et al., 1971; Jerauld et al., 1983)

$$\frac{\partial n}{\partial \bar{t}} = -\frac{\partial(R(\bar{t})n)}{\partial r} - \frac{n}{\tau} + \delta(r-0)Q(\bar{t})$$
$$\frac{dc}{d\bar{t}} = \frac{(c_0-\rho)}{\bar{\epsilon}\tau} + \frac{(\rho-c)}{\tau} + \frac{(\rho-c)}{\bar{\epsilon}}\frac{d\bar{\epsilon}}{d\bar{t}} \qquad (6)$$

where $n(r,\bar{t})$ is the number of crystals of radius $r \in [0, \infty)$ at time $\bar{t}$ per unit volume of suspension, τ is the residence time, c is the solute concentration in the crystallizer, c_0 is the solute concentration in the feed, and $\bar{\epsilon} = 1 - \int_0^\infty n(r,\bar{t})(4/3)\pi r^3 dr$ is the volume of liquid per unit volume of suspension. $R(\bar{t})$ is the growth rate, $\delta(r-0)$ is the standard Dirac function, and $Q(\bar{t})$ is the nucleation rate. The term $\delta(r-0)Q(\bar{t})$ accounts for the production of crystals of infinitesimal (zero) size via nucleation. $R(\bar{t})$ and $Q(\bar{t})$ are assumed to follow McCabe's law and Volmer's nucleation law, respectively

$$R(\bar{t}) = k_1(c-c_s), \quad Q(\bar{t}) = \bar{\epsilon}k_2 e^{-k_3/[(c/c_s)-1]^2} \qquad (7)$$

where k_1, k_2, and k_3 are constants and c_s is the concentration of solute at saturation. Using the expressions for $Q(\bar{t})$ and $R(\bar{t})$, the system of Eq. 6 can be equivalently written as

$$\frac{\partial n}{\partial \bar{t}} = -k_1(c-c_s)\frac{\partial n}{\partial r} - \frac{n}{\tau} + \delta(r-0)\bar{\epsilon}k_2 e^{-k_3/[(c/c_s)-1]^2}$$
$$\frac{dc}{d\bar{t}} = \frac{(c_0-\rho)}{\bar{\epsilon}\tau} + \frac{(\rho-c)}{\tau} + \frac{(\rho-c)}{\bar{\epsilon}}\frac{d\bar{\epsilon}}{d\bar{t}} \qquad (8)$$

To study the dynamic behavior of the crystallizer in question, a second-order accurate finite difference scheme with 1,000 discretization points was used to obtain the solution of the system of Eq. 6. The values of the process parameters used in the simulations are given in Tables 1 and 2. Figure 2 shows the open-loop oscillatory profiles of the total crystal concentration and total crystal size, respectively. It is clear that the

Table 1. Process Parameters

$c_0 = 1{,}000.0$	$kg \cdot m^{-3}$
$c_s = 980.2$	$kg \cdot m^{-3}$
$\rho = 1{,}770.0$	$kg \cdot m^{-3}$
$\tau = 1.0$	h
$k_1 = 5.065 \times 10^{-2}$	$mm \cdot m^3 \cdot kg^{-1} \cdot h^{-1}$
$k_2 = 7.958$	$mm^{-3} \cdot h^{-1}$
$k_3 = 1.217 \times 10^{-3}$	

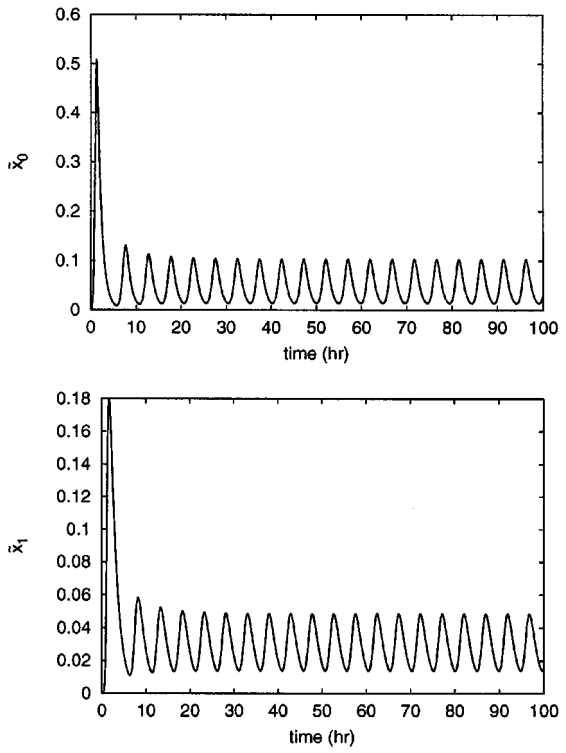

Figure 2. Open-loop crystal concentration (top) and total crystal size (bottom); distributed parameter model.

crystallizer exhibits highly oscillatory behavior, which is the result of the interplay between growth and nucleation caused by the relative nonlinearity of the nucleation rate as compared to growth rate (compare the nonlinear dependence of $Q(\bar{t})$ and $R(\bar{t})$ on c in Eq. 7). To establish that the dynamics of the crystallizer are characterized by a small number of degrees of freedom, the method of moments is applied to the system of Eq. 6 to derive an approximate ODE model. This is possible because the nucleation and growth rates are assumed to be independent of particle size which allows closure of the moment equations (see Eq. 12 below). It is noted that the method of moments has been extensively used in the past to analyze the dynamics of particulate processes [see, for example, Hulburt and Katz (1964) and Pratsinis (1988)].

Defining the νth moment of $n(r,\bar{t})$ as

$$\mu_\nu = \int_0^\infty r^\nu n(r,\bar{t})\,dr, \quad \nu = 0, \ldots, \qquad (9)$$

multiplying the population balance in Eq. 8 by r^ν, and integrating over all particle sizes, the following system of infinite

Table 2. Dimensionless Variables

$\sigma = k_1\tau(c_0 - c_s)$	= 1.0 mm
$Da = 8\pi\sigma^3 k_2 \tau$	= 200.0
$F = k_3 c_s^2/(c_0 - c_s)^2$	= 3.0
$\alpha = (\rho - c_s)/(c_0 - c_s)$	= 40.0

ordinary differential equations, which describes the rate of change of the moments of the PSD and the solute concentration, is obtained

$$\frac{d\mu_0}{dt} = -\frac{\mu_0}{\tau} + \left(1 - \frac{4}{3}\pi\mu_3\right) k_2 e^{-k_3/[(c/c_s)-1]^2}$$

$$\frac{d\mu_\nu}{dt} = -\frac{\mu_\nu}{\tau} + \nu k_1 (c - c_s)\mu_{\nu-1}, \quad \nu = 1, 2, 3, \ldots,$$

$$\frac{dc}{dt} = \frac{c_0 - c - 4\pi\tau(c - c_s)\mu_2(\rho - c)}{\tau\left(1 - \frac{4}{3}\pi\mu_3\right)} \tag{10}$$

Introducing the following set of dimensionless variables and parameters

$$t = \frac{\bar{t}}{\tau}, \quad \tilde{x}_0 = 8\pi\sigma^3\mu_0, \quad \tilde{x}_1 = 8\pi\sigma^2\mu_1, \quad \tilde{x}_2 = 4\pi\sigma\mu_2,$$

$$\tilde{x}_3 = \frac{4}{3}\pi\mu_3, \ldots, \quad \sigma = k_1\tau(c_0 - c_s), \quad Da = 8\pi\sigma^3 k_2\tau,$$

$$F = \frac{k_3 c_s^2}{(c_0 - c_s)^2}, \quad \alpha = \frac{(\rho - c_s)}{(c_0 - c_s)}, \quad \tilde{y} = \frac{(c - c_s)}{(c_0 - c_s)} \tag{11}$$

the following dimensionless system is obtained

$$\frac{d\tilde{x}_0}{dt} = -\tilde{x}_0 + (1 - \tilde{x}_3) Da e^{-F/\tilde{y}^2}$$

$$\frac{d\tilde{x}_1}{dt} = -\tilde{x}_1 + \tilde{y}\tilde{x}_0$$

$$\frac{d\tilde{x}_2}{dt} = -\tilde{x}_2 + \tilde{y}\tilde{x}_1$$

$$\frac{d\tilde{x}_3}{dt} = -\tilde{x}_3 + \tilde{y}\tilde{x}_2$$

$$\frac{d\tilde{x}_\nu}{dt} = -\tilde{x}_\nu + \tilde{y}\tilde{x}_{\nu-1}, \quad \nu = 4, \ldots,$$

$$\frac{d\tilde{y}}{dt} = \frac{1 - \tilde{y} - (\alpha - \tilde{y})\tilde{y}\tilde{x}_2}{1 - \tilde{x}_3} \tag{12}$$

On the basis of the system of Eq. 12, it is clear that the moments of order four and higher do not affect those of order three and lower, and, moreover, the state of the infinite-dimensional system

$$\frac{d\tilde{x}_\nu}{dt} = -\tilde{x}_\nu + \tilde{y}\tilde{x}_{\nu-1}, \quad \nu = 4, \ldots, \tag{13}$$

is bounded when x_3 and y are bounded, and it converges to a globally exponentially stable equilibrium point when $\lim_{t\to\infty} x_3 = c_1$ and $\lim_{t\to\infty} \tilde{y} = c_2$, where c_1, c_2 are constants. This implies that the dominant dynamics (that is, dynamics associated with eigenvalues that are close to the imaginary axis) of the process of Eq. 8 can be adequately captured by

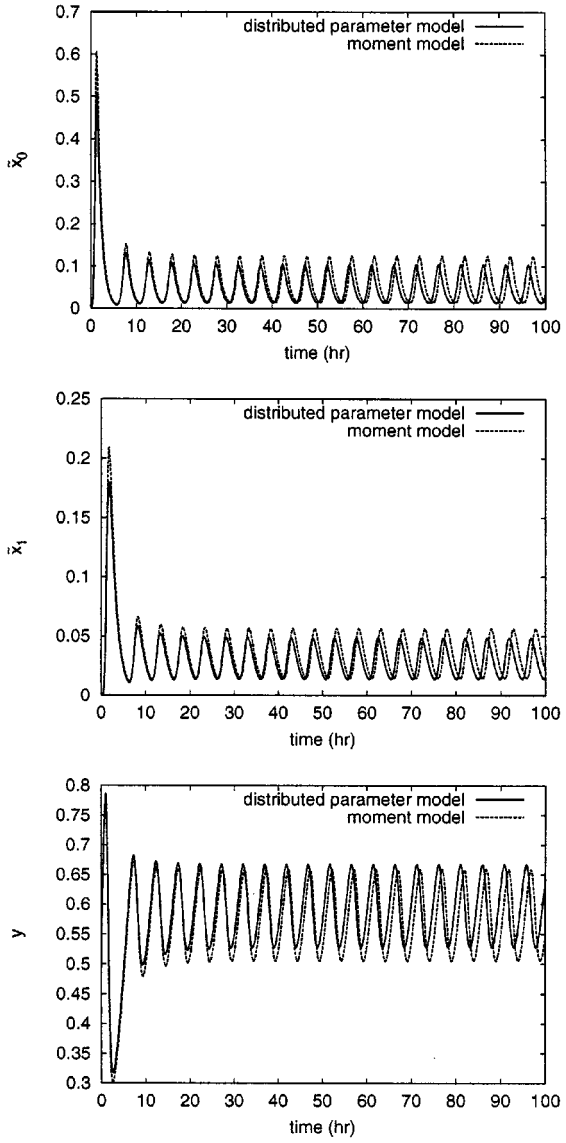

Figure 3. Open-loop crystal concentration (top), total crystal size (middle), and solute concentration (bottom) obtained from the distributed parameter model and the moment model.

the following fifth-order moment model

$$\frac{d\tilde{x}_0}{dt} = -\tilde{x}_0 + (1 - \tilde{x}_3) Da e^{-F/\tilde{y}^2}$$

$$\frac{d\tilde{x}_1}{dt} = -\tilde{x}_1 + \tilde{y}\tilde{x}_0$$

$$\frac{d\tilde{x}_2}{dt} = -\tilde{x}_2 + \tilde{y}\tilde{x}_1$$

$$\frac{d\tilde{x}_3}{dt} = -\tilde{x}_3 + \tilde{y}\tilde{x}_2$$

$$\frac{d\tilde{y}}{dt} = \frac{1 - \tilde{y} - (\alpha - \tilde{y})\tilde{y}\tilde{x}_2}{1 - \tilde{x}_3} \tag{14}$$

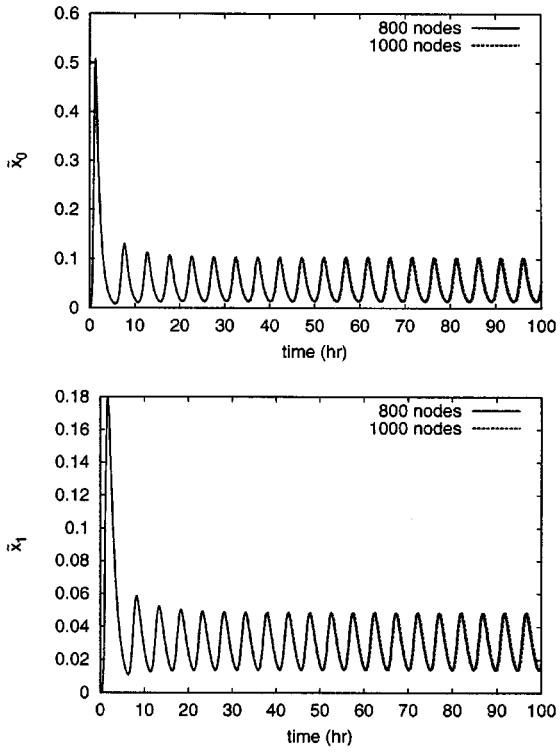

Figure 4. Effect of the number of discretization points on crystal concentration (top) and total crystal size (bottom); distributed parameter model.

The ability of the above fifth-order moment model to reproduce the dynamics, and to some extent the solutions, of the distributed model of Eq. 6 is shown in Figure 3, where the profiles of the total particle concentration generated by the two models are compared (both models start from the same initial conditions). Even though the discrepancy of the total particle concentration profiles predicted by the two models increases with time (this is expected due to the open-loop instability of the process; see remark 7 below), it is clear that the fifth-order moment model of Eq. 14 provides a very good approximation of the distributed model of Eq. 6, thereby establishing that the dominant dynamics of the system of Eq. 8 are low-dimensional and motivating the use of the moment model for nonlinear controller design (see the section Application to a Continuous Crystallizer for the design and implementation of a nonlinear controller based on the fifth-order model of Eq. 14).

Remark 3. The stability properties of the fifth-order model of Eq. 14 have been thoroughly studied in Jerauld et al. (1983) [see also Lei et al. (1971)], where it has been shown that the global phase space of this model consists of a unique unstable steady state surrounded by a stable periodic orbit, and that the linearization of the system of Eq. 6 around the unstable steady state includes two isolated complex conjugate eigenvalues with a positive real part. For the parameters of Table 1, the unique unstable steady state is $\tilde{x}_0 = 0.047$, $\tilde{x}_1 = 0.028$, $\tilde{x}_2 = 0.017$, $\tilde{x}_3 = 0.01$, $\tilde{y} = 0.5996$.

Remark 4. We note that even though the number of discretization points, 1,000, used to solve the system of Eq. 6 is very large (owing to the poor convergence properties of the finite-difference scheme), the computation of an accurate (that is, independent of the discretization) solution is critical for the thorough evaluation of the performance of a nonlinear feedback controller synthesized on the basis of a low-order approximation of the distributed parameter system of Eq. 6 (see the section Application to a Continuous Crystallizer for closed-loop system simulations under nonlinear low-order output feedback control). The adequacy of 1,000 discretization points to yield an accurate solution is established in Figure 4, where the profiles of the total crystal concentration and total crystal size for 800 and 1,000 discretization points are compared and are shown to be almost identical.

Remark 5. Despite the fact that the model of Eq. 6 consists of a first-order hyperbolic PDE (population balance) coupled with a nonlinear integro-differential equation (solute mass balance), it is evident from the above dynamical analysis, and the results of the simulation study, that its open-loop dynamic behavior is completely different than the one usually exhibited by systems of first-order hyperbolic PDEs (which arise in the modeling of convection-reaction processes). More specifically, the dominant dynamic behavior of the system of Eq. 6 is characterized by a small number of degrees of freedom (and, thus, it can be described by low-order ODE systems). On the other hand, first-order hyperbolic PDE systems involve spatial differential operators whose eigenvalues cluster along vertical, or nearly vertical, asymptotes in the complex plane, and, therefore, they do not exhibit low-dimensional dynamic behavior. This fundamental difference on the nature of the dynamic behavior between first-order hyperbolic PDE systems and particulate process models motivates employing fundamentally different approaches for designing controllers for such systems. In particular, for first-order hyperbolic PDEs, the controller design problem is addressed directly on the basis of the PDE system (see Christofides and Daoutidis (1996a) for results on nonlinear control), while for systems of Eqs. 1–2, the controller design problem will be addressed on the basis of low-order approximations that capture the dominant dynamics, as outlined in the next section.

Remark 6. When a fines trap is used to remove fines, small crystals, from the crystal magma [see Lei et al. (1971) and Randolph et al. (1987) for a detailed description of crystallizer with fines trap], the model of the crystallizer takes the following form (Lei et al., 1971)

$$\frac{\partial n}{\partial \bar{t}} = -k_1(c-c_s)\frac{\partial n}{\partial r} - \frac{n}{\tau} - \bar{h}(r)\frac{n}{\tilde{\tau}} + \delta(r-0)\bar{\epsilon}k_2 e^{-\{k_3/[(c_1/c_s)-1]^2\}}$$

$$\frac{dc}{d\bar{t}} = \frac{(c_0-\rho)}{\bar{\epsilon}\tau} + \frac{(\rho-c)}{\tau} + \frac{(\rho-c)}{\bar{\epsilon}}\frac{d\bar{\epsilon}}{d\bar{t}} \qquad (15)$$

where $1/\tilde{\tau} = F_0/V$ is the rate at which crystals are circulated through the fines trap (F_0 is the fines recirculation rate, and V is the active volume of the crystallizer) and $\bar{h}(r)$ expresses the desired selection curve for fines destruction (classifica-

tion function). For example, if we desire to remove crystals of size r_m and smaller, then $\bar{h}(r)$ has the form

$$\bar{h}(r) = \begin{bmatrix} 1, & \text{for } r \le r_m \\ 0, & \text{for } r > r_m \end{bmatrix} \tag{16}$$

For the distributed parameter model of Eq. 15 with the above expression for $\bar{h}(r)$, one can easily show that a direct application of the method of moments leads to an unclosed set of moments equations, thereby implying the need of using a general model reduction procedure for particulate processes (see the section Nonlinear Model Reduction of Particulate Process Models).

Methodological Framework for Control of Particulate Processes

Owing to its distributed parameter nature, the system of Eqs. 1–2 cannot be directly used as the basis for the synthesis of low-order nonlinear controllers that can be implemented. This fact, together with the realization that the dominant dynamics of particulate processes are characterized by a small number of degrees of freedom, motivates employing the following methodology for the synthesis of low-order nonlinear output feedback controllers for systems of the form of Eqs. 1–2:

(1) Initially, the method of weighted residuals is used to derive a nonlinear, possibly high-order, ODE system that accurately reproduces the solutions and dynamics of the system of Eqs. 1–2. Then, a procedure based on the concept of approximate inertial manifold is employed for the construction of low-order ODE systems that accurately reproduce the dominant dynamics of the large-scale ODE system obtained by the method of weighted residuals. The asymptotic validity of the ODE approximation is established by using results from perturbation theory.

(2) Then, the low-order ODE approximation of the system of Eqs. 1–2 is used as the basis for the synthesis via geometric control methods of nonlinear output feedback controllers that stabilize the closed-loop ODE system and enforce output tracking.

(3) Finally, the resulting closed-loop system (particulate process model of Eqs. 1–2 and controller) is analyzed to derive conditions that guarantee that the desired stability and set point tracking properties are enforced in the infinite-dimensional closed-loop system.

Nonlinear Model Reduction of Particulate Process Models

In this section, we introduce a general methodology for deriving low-order ODE systems that accurately reproduce the dominant dynamics of the nonlinear integro-differential equation system of Eqs. 1–2. The proposed model reduction methodology exploits the low-dimensional behavior of the dominant dynamics of the system of Eqs. 1–2 and is based on a combination of the method of weighted residuals with the concept of approximate inertial manifold.

Method of weighted residuals

We initially use the method of weighted residuals to construct a nonlinear, possibly high-order, ODE system that accurately reproduces the solutions and dynamics of the distributed parameter system of Eqs. 1–2. The central idea of the method of weighted residuals [see Ramkrishna (1985) for a comprehensive review of results on the use of this method for solving population balance equations] is to approximate the exact solution of $n(r,t)$ by an infinite series of orthogonal basis functions defined on the interval $[0, r_{\max})$ with time-varying coefficients, substitute the series expansion into Eq. 1 to form the residual, and then force the residual to be orthogonal to a complete set of weighted functions (that is, the inner product of the residual with a complete set of weighting functions in $L_2[0, r_{\max})$ is set equal to zero) to compute a set of ODEs which describe the rate of change of the time-varying coefficients of the series expansion of the solution.

Specifically, we consider an orthogonal set of basis functions $\phi_k(r)$, where $r \in [0, r_{\max})$, $k = 1, \ldots, \infty$, and expand the PSD function $n(r,t)$ in an infinite series in terms of $\phi_k(r)$ as follows

$$n(r,t) = \sum_{k=1}^{\infty} a_k(t)\phi_k(r) \tag{17}$$

where $a_k(t)$ are time-varying coefficients. Substituting Eq. 17 into Eqs. 1–2, we get

$$\begin{aligned} &\sum_{k=1}^{\infty} \phi_k(r)\frac{\partial a_k(t)}{\partial t} \\ &\quad = -\sum_{k=1}^{\infty} a_k(t)\frac{\partial\left[G(x,r)\phi_k(r)\right]}{\partial r} + w\left[\sum_{k=1}^{\infty} a_k(t)\phi_k(r), x, r\right] \\ &\dot{x} = f(x) + g(x)u(t) + A\int_0^{r_{\max}} a\left[\sum_{k=1}^{\infty} a_k(t)\phi_k(r), r, x\right] dr \end{aligned} \tag{18}$$

Multiplying the population balance with the weighting functions $\psi_\nu(r)$, and integrating over the entire particle-size spectrum (that is, taking inner product in $L_2[0, r_{\max})$ with the weighting functions), the following set of infinite ODEs is obtained

$$\begin{aligned} &\int_0^{r_{\max}} \psi_\nu(r) \sum_{k=1}^{\infty} \phi_k(r)\frac{\partial a_k(t)}{\partial t} dr \\ &\quad = -\sum_{k=1}^{\infty} a_k(t)\int_0^{r_{\max}} \psi_\nu(r)\frac{\partial\left[G(x,r)\phi_k(r)\right]}{\partial r} dr \\ &\qquad + \int_0^{r_{\max}} \psi_\nu(r) w\left[\sum_{k=1}^{\infty} a_k(t)\phi_k(r), x, r\right] dr, \quad \nu = 1, \ldots, \infty \\ &\dot{x} = f(x) + g(x)u(t) + A\int_0^{r_{\max}} a\left[\sum_{k=1}^{\infty} a_k(t)\phi_k(r), r, x\right] dr \end{aligned} \tag{19}$$

Truncating the series expansion of $n(r,t)$ up to order N and keeping the first N equations (that is, $\nu = 1, \ldots, N$), the infinite-dimensional system of Eq. 19 reduces to the following finite set of ODEs

$$\int_0^{r_{\max}} \psi_\nu(r) \sum_{k=1}^{N} \phi_k(r) \frac{\partial a_{kN}(t)}{\partial t} dr$$
$$= -\sum_{k=1}^{N} a_{kN}(t) \int_0^{r_{\max}} \psi_\nu(r) \frac{\partial \left[G(x_N, r) \phi_k(r) \right]}{\partial r} dr$$
$$+ \int_0^{r_{\max}} \psi_\nu(r) w \left[\sum_{k=1}^{N} a_{kN}(t) \phi_k(r), x_N, r \right] dr, \quad \nu = 1, \ldots, N$$

$$\dot{x}_N = f(x_N) + g(x_N) u(t) + A \int_0^{r_{\max}} a \left[\sum_{k=1}^{N} a_{kN}(t) \phi_k(r), r, x_N \right] dr$$

$$y_i(t) = h_i \left[\int_0^{r_{\max}} c_\kappa \sum_{k=1}^{N} a_{kN}(t) \phi_k(r) dr, x_N \right], \quad i = 1, \ldots, m, \ \kappa = 1, \ldots, l \quad (20)$$

where x_N and a_{kN} are the approximations of x and a_k obtained by an Nth order truncation. From Eq. 20, it is clear that the form of the ODEs that describe the rate of change of $a_{kN}(t)$ depends on the choice of the basis and weighting functions, as well as on N. The basis and weighting functions determine the type of weighted residual method being used (see Remarks 8 and 9 below).

Proposition 1 that follows establishes a convergence property for the discrepancy between the solutions of the particulate process model of Eqs. 1–2 and the approximation of Eq. 20 for sufficiently large N.

Proposition 1. Consider the system of Eqs. 1–2 with $u(t) \equiv 0$ and assume that n and $\partial n/\partial r$ are continuous functions of r. Suppose also that the system of Eq. 20 is locally exponentially stable for any N. Then, there exists an N sufficiently large so that $\forall t \geq 0$

$$n(r,t) = n_N(r,t) + O[\epsilon(N)]$$
$$x(t) = x_N(t) + O[\epsilon(N)] \quad (21)$$

where $\epsilon(N)$ is a small positive real number that depends on N and satisfies $\lim_{N \to \infty} \epsilon(N) = 0$, and $n_N(r,t) = \sum_{k=1}^{N} a_{kN}(t) \phi_k(r)$ is the approximation of $n(r,t)$ which is obtained by solving Eq. 20 with $u(t) \equiv 0$.

Remark 7. The assumption that the system of Eq. 20 (and, thus, the system of Eqs. 1–2) is locally exponentially stable is necessary in order to prove that the estimates of Eq. 21 hold for all times. When the system of Eq. 20 is not exponentially stable, one can only prove that the estimates of Eq. 21 hold for $t \in [0, \tau]$ where τ is a positive real number of $O(1)$ (see simulations results in the subsection on the dynamics of particulate processes for a verification of this fact). Furthermore, the convergence result can be shown for the $L_2[0,\infty)$ norm of the difference between the solution of the population balance $n(r,t)$ and its approximation of Eq. 17, that is, for all $t \in [0,\infty)$

$$\lim_{N \to \infty} \left\| n(r,t) - \sum_{k=1}^{N} a_{kN}(t) \phi_k(r) \right\|_2 = 0 \quad (22)$$

Remark 8. The method of weighted residuals reduces to the method of moments when the basis functions are chosen to be Laguerre polynomials and the weighting functions are chosen as $\psi_\nu = r^\nu$. The moments of the PSD are defined as

$$\mu_\nu = \int_0^\infty r^\nu n(r,t) dr, \quad \nu = 0, \ldots, \infty \quad (23)$$

and the moment equations can be directly generated from the population balance model by multiplying it by r^ν, $\nu = 0, \ldots, \infty$ and integrating from 0 to ∞. The procedure of forming moments of the population balance equation very often leads to terms that may not reduce to moments, terms that include fractional moments, or to an unclosed set of moment equations. To overcome this problem, the PSD is expanded in terms of Laguerre polynomials defined in $L_2[0,\infty)$ and the series solution is used to close the set of moment equations (this procedure can be used for models of crystallizers with fines trap; see Eqs. 15–16).

Remark 9. When the number of basis functions $\phi_k(r)$ required to obtain a good approximation (measured in a desired norm) of the solution of the population balance is small, then the weighting functions are usually chosen (Rawlings et al., 1993) to be identical to the basis functions, in which case the method of weighted residuals reduces to Galerkin's method.

Remark 10. When a ''good''(in the sense of leading to the derivation of an ODE system of desired accuracy whose dimension is not extremely high) set of basis functions $\phi_k(r)$ cannot be found within the standard basis function sets, one can compute a set of empirical eigenfunctions by applying the Karhunen-Loéve expansion (Fukunaga, 1990; Holmes et al., 1996; Shvartsman and Kevrekidis, 1998) (also known as proper orthogonal decomposition) on an approximate ensemble of solutions of the particulate process model of Eqs. 1–2, which are obtained from detailed finite-difference discretizations.

Inertial manifold and approximate inertial manifold

The system of Eq. 20 was obtained from a direct application of the method of weighted residuals (with arbitrary basis functions) to the system of Eqs. 1–2 and, thus, may be of very high order in order to provide an accurate description of the dominant dynamics of the particulate process model. High-dimensionality of the system of Eq. 20 leads to complex controller design and high-order controllers, which cannot be readily implemented in practice. To circumvent these problems, we exploit the low-dimensional behavior of the dominant dynamics of particulate processes and use an approach based on the concept of inertial manifold to derive low-order ODE systems that accurately describe the dominant dynamics of the system of Eq. 20. The concept of inertial manifold is an appropriate tool for model reduction, because if the

trajectories of the system of Eq. 20 are on the manifold, then this system is *exactly* described by a low-order system.

We begin with the definition of the concept of inertial manifold, and we continue with the concept of approximate inertial manifold. To this end, we exploit the orthogonality of the basis functions $\phi_k(r)$ to uniquely split

$$n_N = \sum_{k=1}^{p} a_{kN}(t)\phi_k(r) + \sum_{k=p+1}^{N} a_{kN}(t)\phi_k(r) =: n_p + n_q \tag{24}$$

where the first p eigenmodes are associated with the dominant (possibly unstable) dynamics of the system of Eq. 20, and the remaining q eigenmodes are associated with exponentially stable dynamics.

Introducing the vector notation $a_N = [a_{1N} \ \cdots \ a_{NN}]$ and defining the new vectors of state variables $\tilde{x} = [a_{sN}^T \ x_N^T]^T$, $a_{sN} = [a_{1N} \ \cdots \ a_{pN}]^T$ and $a_{fN} = [a_{(p+1)N} \ \cdots \ a_{NN}]^T$, the system of Eq. 20 can be written as

$$\begin{aligned} \dot{a}_{fN} &= \bar{f}_q(a_{fN}, \tilde{x}) \\ \dot{\tilde{x}} &= \tilde{f}(\tilde{x}, a_{fN}) + \tilde{g}(\tilde{x}, a_{fN})u \\ y_i &= \tilde{h}_i(\tilde{x}, a_{fN}), \quad i = 1, \ldots, m \end{aligned} \tag{25}$$

where the explicit expression of $\bar{f}_q(a_{fN}, \tilde{x})$, $\tilde{f}(\tilde{x}, a_{fN})$, $\tilde{g}(\tilde{x}, a_{fN})$, $\tilde{h}_i(\tilde{x}, a_{fN})$ can be obtained by comparing Eq. 20 and Eq. 25 and will be omitted for brevity. Assuming that $\bar{f}_q(a_{fN}, \tilde{x}) = \tilde{A}a_{fN} + \tilde{f}_q(a_{fN}, \tilde{x})$ where $\tilde{A}$ is a Hurwitz matrix and $\tilde{f}_q(a_{fN}, \tilde{x})$ is a nonlinear vector function which does not include linear terms (this assumption is made to simplify the development and can be readily relaxed), the system of Eq. 25 can be written as

$$\begin{aligned} \dot{a}_{fN} &= \tilde{A}a_{fN} + \tilde{f}_q(a_{fN}, \tilde{x}) \\ \dot{\tilde{x}} &= \tilde{f}(\tilde{x}, a_{fN}) + \tilde{g}(\tilde{x}, a_{fN})u \\ y_i &= \tilde{h}_i(\tilde{x}, a_{fN}), \quad i = 1, \ldots, m \end{aligned} \tag{26}$$

For the above system, an inertial manifold $\mathfrak{M}$ is a subset of $\mathbb{R}^{N+n}$, which satisfies the following properties (Temam, 1988):

(a) $\mathfrak{M}$ is a finite-dimensional Lipschitz manifold;

(b) $\mathfrak{M}$ is a graph of a Lipschitz function $\Sigma(\tilde{x})$ mapping $\mathbb{R}^{p+n}$ into $\mathbb{R}^q$ and for every solution $\tilde{x}(t)$, $a_{fN}(t)$ of Eq. 26 with $a_{fN}(0) = \Sigma[\tilde{x}(0)]$; then

$$a_{fN}(t) = \Sigma[\tilde{x}(t)], \quad \forall t \geq 0 \tag{27}$$

(c) $\mathfrak{M}$ attracts every trajectory exponentially.

The evolution of the state $a_{fN}(t)$ on $\mathfrak{M}$ is given by Eq. 27, while the evolution of the state $\tilde{x}$ is governed by the following $(p+n)$-order system

$$\begin{aligned} \dot{\tilde{x}} &= \tilde{f}[\tilde{x}, \Sigma(\tilde{x})] + \tilde{g}[\tilde{x}, \Sigma(\tilde{x})]u \\ y_i &= \tilde{h}_i[\tilde{x}, \Sigma(\tilde{x})], \quad i = 1, \ldots, m \end{aligned} \tag{28}$$

Differentiating Eq. 27 and utilizing Eq. 26, $\Sigma(\tilde{x})$ can be computed as the solution of the following partial differential equation

$$\frac{\partial \Sigma}{\partial \tilde{x}}\{\tilde{f}[\tilde{x}, \Sigma(\tilde{x})] + \tilde{g}[\tilde{x}, \Sigma(\tilde{x})]u\} = \tilde{A}\Sigma(\tilde{x}) + \tilde{f}_q[\Sigma(\tilde{x}), \tilde{x}] \tag{29}$$

which $\Sigma(\tilde{x})$ has to satisfy for all $\tilde{x} \in \mathbb{R}^{p+n}$. From the structure of Eq. 29, it is obvious that the computation of the explicit form of $\Sigma(\tilde{x})$ is a very difficult (if not impossible) task in most practical applications. To overcome this problem, and since the dynamics of the a_{fN} modes are stable and faster than the ones of the $\tilde{x}$ modes (note that the number of unstable eigenvalues of the system of Eqs. 1–2 is finite, and by assumption, all the unstable eigenvalues are included in the $\tilde{x}$ subsystem), we obtain $\Sigma(\tilde{x})$ by setting $\dot{a}_{fN} = (\partial\Sigma/\partial\tilde{x})[\tilde{f}(\tilde{x}, \Sigma) + \tilde{g}(\tilde{x}, \Sigma)u] \equiv 0$ and solving the equation

$$\tilde{A}\Sigma(\tilde{x}) + \tilde{f}_q[\Sigma(\tilde{x}), \tilde{x}] = 0 \tag{30}$$

using a standard successive approximation (fixed point) algorithm (Foias and Témam, 1988) [see also Shvartsman and Kevrekidis (1998)]

$$\begin{aligned} &\tilde{\Sigma}_{\kappa+1}(\tilde{x}) = -\tilde{A}^{-1}\tilde{f}_q[\tilde{\Sigma}_\kappa(\tilde{x}), \tilde{x}], \quad \kappa = 0, \ldots, \bar{l}, \ \tilde{\Sigma}_0(\tilde{x}) = 0 \\ &\tilde{a}_{fN} = \tilde{\Sigma}_{\bar{l}+1}(\tilde{x}) \end{aligned} \tag{31}$$

where $\tilde{\Sigma}_{\bar{l}+1}(\tilde{x})$ is an approximation of $\Sigma(\tilde{x})$ (called approximate inertial manifold) and $\tilde{a}_{fN}$ is the approximation of a_{fN}. Substituting $\tilde{\Sigma}_{\bar{l}+1}(\tilde{x})$ into the system of Eq. 28, the following $(p+n)$-order approximation of the particulate process model is obtained

$$\begin{aligned} \dot{\tilde{x}} &= \tilde{f}[\tilde{x}, \tilde{\Sigma}_{\bar{l}+1}(\tilde{x})] + \tilde{g}[\tilde{x}, \tilde{\Sigma}_{\bar{l}+1}(\tilde{x})]u =: \tilde{f}(\tilde{x}) + \tilde{g}(\tilde{x})u \\ y_{s_i} &= \tilde{h}_i[\tilde{x}, \tilde{\Sigma}_{\bar{l}+1}(\tilde{x})] =: \tilde{h}_i(\tilde{x}), \quad i = 1, \ldots, m \end{aligned} \tag{32}$$

where the subscript s in the controlled output y_{s_i} denotes that this controlled output is associated with an approximate low-order ODE system (refer to Eq. 3 for the formulation of y_i for the distributed parameter model).

Proposition 2 that follows establishes that the local stability properties and solutions for large times of the systems Eq. 32 and Eq. 20 are identical. The proof is given in the Appendix.

Proposition 2. Suppose that the sequence of Eq. 31 for the construction of $\tilde{\Sigma}_{\bar{l}+1}(\tilde{x})$ converges for $\bar{l}$ sufficiently large (that is, for any $\tilde{\epsilon}$, there exists an $\bar{l}^*$ such that if $\bar{l} \geq \bar{l}^*$, then $|\Sigma(\tilde{x}) - \tilde{\Sigma}_{\bar{l}+1}(\tilde{x})| \leq \tilde{\epsilon}$). Suppose also that the $(p+n)$-order system of Eq. 32 with $u(t) \equiv 0$ is locally exponentially stable. Then, the $(N+n)$-order system of Eq. 20 with $u(t) \equiv 0$ is locally exponentially stable and $\lim_{t\to\infty}\|n_N - \bar{n}_N\|_2 = O[\tilde{\epsilon}(\bar{l})]$, where $\bar{n}_N = \sum_{k=1}^{p}\tilde{a}_{kN}(t)\phi_k(r) + \sum_{k=p+1}^{N}\tilde{\Sigma}_{\bar{l}+1}(\tilde{x})\phi_k(r)$ [$\tilde{a}_{kN}(t)$ is the solution obtained from the system of Eq. 32] and $\tilde{\epsilon}(\bar{l})$

is a small positive real number that depends on $\bar{l}$ and satisfies $\lim_{\bar{l}\to\infty}\tilde{\epsilon}(\bar{l})=0$.

Remark 11. We note that even though many particulate processes exhibit low-dimensional dynamic behavior, the delicate mathematical question of rigorously establishing existence of inertial manifolds for particulate process models, at this stage, is unresolved. Such a question has been positively answered for certain classes of diffusion-reaction systems and the Kuramoto-Sivashinsky equation [see Temam (1988) for details].

Remark 12. The expression of the approximate inertial manifold $\tilde{\Sigma}_{\bar{l}+1}(\tilde{x})$ of Eq. 31 (where $\bar{l}$ is chosen based on the desired degree of approximation) was originally proposed in Foias and Témam (1988) and is called the steady manifold. Also refer to Christofides and Daoutidis (1996b) and Shvartsman and Kevrekidis (1998) for alternative expressions of $\tilde{\Sigma}(\tilde{x})$, as well as detailed computational studies that show that the use of approximate inertial manifolds leads to accurate low-order ODE approximations and low-order controllers for diffusion-reaction systems described by parabolic partial differential equations.

Remark 13. For $\Sigma(\tilde{x})=0$, we obtain the following $(p+n)$-order approximation of the particulate process model

$$\dot{a}_{sN}=\bar{f}_p(a_{sN},0,x_N)$$

$$\dot{x}_N=f(x_N)+g(x_N)u(t)+A\int_0^{r_{\max}}a(n_p,x_N,r)\,dr \quad (33)$$

The above system is identical to the one obtained by a direct application of the method of weighted residuals to the particulate process model of Eqs. 1–2 (Eq. 20 with $N=p$).

Nonlinear Output Feedback Control of Particulate Processes

In this section, the system of Eq. 32 is used to synthesize a nonlinear finite-dimensional output feedback controller that guarantees stability and enforces output tracking in the closed-loop ODE system and to establish that the same controller exponentially stabilizes the closed-loop particulate process model. The output feedback controller is constructed through a standard combination of a state feedback controller with a state observer. The state feedback controller is synthesized via geometric control methods, and the state observer is an extended Luenberger-type observer. This section begins with some preliminaries, which will be used to state the controller synthesis result.

Preliminaries

Referring to the system of Eq. 32, we define the relative order of the output y_{s_i} with respect to the vector of manipulated inputs u as the smallest integer r_i for which

$$\left[L_{\tilde{g}_1}L_{\tilde{f}}^{r_i-1}\tilde{h}_i(\tilde{x})\ \cdots\ L_{\tilde{g}_m}L_{\tilde{f}}^{r_i-1}\tilde{h}_i(\tilde{x})\right]\not\equiv[0\ \cdots\ 0] \quad (34)$$

where $\tilde{g}_i$ is the ith vector of the matrix $\tilde{g}$, or $r_i=\infty$ if such an integer does not exist. We also define the characteristic matrix

$$C(\tilde{x})=\begin{bmatrix} L_{\tilde{g}_1}L_{\tilde{f}}^{r_1-1}\tilde{h}_1(\tilde{x}) & \cdots & L_{\tilde{g}_m}L_{\tilde{f}}^{r_1-1}\tilde{h}_1(\tilde{x}) \\ L_{\tilde{g}_1}L_{\tilde{f}}^{r_2-1}\tilde{h}_2(\tilde{x}) & \cdots & L_{\tilde{g}_m}L_{\tilde{f}}^{r_2-1}\tilde{h}_2(\tilde{x}) \\ \vdots & \cdots & \vdots \\ L_{\tilde{g}_1}L_{\tilde{f}}^{r_m-1}\tilde{h}_m(\tilde{x}) & \cdots & L_{\tilde{g}_m}L_{\tilde{f}}^{r_m-1}\tilde{h}_m(\tilde{x}) \end{bmatrix} \quad (35)$$

Controller synthesis

We use the nonlinear system of Eq. 32 as a basis for the synthesis, via geometric control methods, of nonlinear state feedback controllers of the general form

$$u=p(\tilde{x})+Q(\tilde{x})v \quad (36)$$

where $p(\tilde{x})$ is a smooth vector function, $Q(\tilde{x})$ is a smooth matrix, and $v\in\mathbb{R}^m$ is the constant reference input vector. The controllers guarantee local exponential stability and enforce a linear input/output response in the system of Eq. 32 [the details on controller synthesis can be found in Isidori (1989) and will be omitted here for brevity].

Under the hypothesis that the system of Eq. 32 is locally observable (that is, its linearization around the desired operating steady state is observable), the practical implementation of a nonlinear state feedback controller of the form of Eq. 36 will be achieved by employing the following nonlinear state observer

$$\frac{d\omega}{dt}=\tilde{f}(\omega)+\tilde{g}(\omega)u+L\left[y-\tilde{h}(\omega)\right] \quad (37)$$

where ω denotes the observer state vector (the dimension of the vector ω is equal to the dimension of $\tilde{x}$ in the system of Eq. 32), $y=[y_1\ y_2\ \cdots\ y_l]^T$ is the measured output vector, and L is a matrix chosen so that the eigenvalues of the matrix $C_L=(\partial\tilde{f}/\partial\omega)_{(\omega=\omega_s)}-L(\partial\tilde{h}/\partial\omega)_{(\omega=\omega_s)}$, where ω_s is the operating steady state, lie in the open left-half of the complex plane. The state observer of Eq. 37 consists of a replica of the system of Eq. 32 plus a linear gain multiplying the discrepancy between the actual and the estimated value of the output, and, therefore, it is an extended Luenberger-type observer.

The state feedback control law of Eq. 36 and the state observer of Eq. 37 can be combined to yield the following nonlinear output feedback control law

$$\frac{d\omega}{dt}=\tilde{f}(\omega)+\tilde{g}(\omega)[p(\omega)+Q(\omega)v]+L\left[y-\tilde{h}(\omega)\right]$$

$$u=p(\omega)+Q(\omega)v \quad (38)$$

Theorem 1 below provides an explicit synthesis formula of the above output feedback control law and conditions that guarantee closed-loop stability and asymptotic output tracking (the proof can be found in the Appendix).

Theorem 1. Suppose that the sequence of Eq. 31 converges for $\bar{l}$ is sufficiently large. Consider the system of Eq.

32 and assume that: (1) it is locally observable in the sense that there exists a matrix L such that $C_L = (1/\mu)\bar{A}$, where μ is a small positive parameter and $\bar{A}$ is a Hurwitz matrix; (2) its characteristic matrix $C(\tilde{x})$ is nonsingular $\forall \tilde{x} \in D \subset \mathbb{R}^{p+n}$; (3) its unforced ($v \equiv 0$) zero dynamics are locally exponentially stable. Finally, consider the particulate process model of Eqs. 1–2 under the nonlinear output feedback controller

$$\frac{d\omega}{dt} = \tilde{f}(\omega) + \tilde{g}(\omega)\left\{\left[\beta_{1r_1} \cdots \beta_{mr_m}\right] C(\omega)\right\}^{-1} \times \left\{v - \sum_{i=1}^{m}\sum_{k=0}^{r_i} \beta_{ik} L_{\tilde{f}}^{k} \tilde{h}_i(\omega)\right\} + L\left(y - \tilde{h}(\omega)\right)$$

$$u = \left\{\left[\beta_{1r_1} \cdots \beta_{mr_m}\right] C(\omega)\right\}^{-1} \left\{v - \sum_{i=1}^{m}\sum_{k=0}^{r_i} \beta_{ik} L_{\tilde{f}}^{k} \tilde{h}_i(\omega)\right\} \tag{39}$$

where the parameters β_{ik} are chosen so that the roots of the equation $\det[B(s)] = 0$ are in the open left-half of the complex plane [$B(s)$ is an $l \times l$ matrix, whose (i, j)th element is of the form $\sum_{k=0}^{r_i} \beta_{jk}^{i} s^k$]. Then, there exists a positive real number μ^* such that if $\mu \in (0, \mu^*]$, the closed-loop system (particulate process model and controller of Eq. 39) is exponentially stable and $\lim_{t\to\infty} |y_i - v_i| = O[\hat{\epsilon}(N + \bar{l})]$, where v_i is the set point for the ith controlled output and $\hat{\epsilon}(N + \bar{l})$ is a small positive real number that depends on N, $\bar{l}$ and satisfies $\lim_{N,\bar{l}\to\infty} \hat{\epsilon}(N + \bar{l}) = 0$.

Remark 14. Regarding the practical application of theorem 1, one has to initially pick an $\bar{l}$ and construct the system of Eq. 32, and then verify assumptions 1, 2, and 3 of the theorem on the basis of this system. If these assumptions are satisfied, the synthesis formula of Eq. 39 can be directly used to derive the explicit form of the controller (see the next section for an application of this procedure to the crystallizer example).

Remark 15. The assumption that $\bar{l}$ is sufficiently large is needed to obtain the stability and closeness of solutions results of proposition 2 for the appropriate approximations of the closed-loop system, while the assumption $C_L = (1/\mu)\bar{A}$, where μ is a small positive parameter and $\bar{A}$ is a Hurwitz matrix, is needed to ensure that the presence of closed-loop system states, which are not included in the model used for controller synthesis, in the state observer does not lead to closed-loop instability. Finally, the assumption that the characteristic matrix $C(\tilde{x})$ is nonsingular is made to simplify the presentation of the controller synthesis results and can be relaxed (see Isidori, 1989, for details).

Remark 16. The exponential stability of the closed-loop system guarantees that in the presence of small initialization errors of the observer states [that is, $\omega(0) \neq \tilde{x}(0)$], and uncertainty in the process parameters and disturbances, the states of the closed-loop system will be bounded. Furthermore, since the number of manipulated inputs and controlled outputs is finite, it is possible to implement a linear error feedback controller (for example, a proportional integral (PI) controller for single-input single-output processes) around the $(y_i - v_i)$, $i = 1, \ldots, l$, loops to ensure asymptotic offsetless output tracking in the closed-loop system in the presence of such uncertainty.

Remark 17. Theorem 1 establishes that a nonlinear output feedback controller which guarantees local exponential stability and output tracking in the finite-dimensional closed-loop system (Eqs. 32–39), continues to enforce the same properties in the infinite-dimensional closed-loop system (Eqs. 1–2–39). This result is intuitively expected because: (a) the dynamics of the modes of the particulate process model which are not taken into account in the controller design (that is, not included in the ODE model of Eq. 32), are locally exponentially stable; and (b) the control action $u(t)$ does not influence the dynamics of the modes which are not taken into account in the controller design [note that $u(t)$ does not enter in the a_{fN}-subsystem of Eq. 25].

Remark 18. The nonlinear controller of Eq. 39 possesses a robustness property with respect to fast and asymptotically stable unmodeled dynamics (that is, the controller enforces exponential stability and output tracking in the closed-loop system despite the presence of additional dynamics in the process, as long as they are stable and sufficiently fast). This property of the controller of Eq. 39 can be rigorously established by analyzing the closed-loop system with the unmodeled dynamics using singular perturbations and is of particulate importance for many practical applications where unmodeled dynamics often occur due to actuator and sensor dynamics, fast process dynamics, and so on.

Application to a Continuous Crystallizer

Controller synthesis

The proposed nonlinear control method is used in this section to stabilize the continuous crystallizer introduced in the second section. Motivated by the fact that the crystallizer with the crystal-size distribution as controlled variable and the solute feed concentration as manipulated input is an approximately controllable system [see Semino and Ray (1995a) for a rigorous controllability analysis], we study two representative control problems: the first one involves manipulating the solute feed concentration $u(t) = c_0 - c_{0s}$, where c_{0s} is the steady-state solute feed concentration, to achieve a crystal-size distribution with desired mass, that is, the controlled output is defined as

$$y(\bar{t}) = 8\pi\sigma^3 \int_0^\infty n(r, \bar{t})\, dr = \tilde{x}_0; \tag{40}$$

and the second one involves manipulating the solute feed concentration to achieve a crystal-size distribution with a desired total particle size, that is, the controlled output is defined as

$$y(\bar{t}) = 8\pi\sigma^2 \int_0^\infty rn(r, \bar{t})\, dr = \tilde{x}_1 \tag{41}$$

Refer to Lei et al. (1971), Randolph et al. (1987), Eaton and Rawlings (1990), and Rawlings et al. (1993) for the use of other manipulated variables including fines destruction rate and crystallizer temperature for the stabilization of crystalliz-

ers (note that the proposed control method can be used for the synthesis of nonlinear controllers when such manipulated inputs are considered).

Including the above specifications for manipulated input and controlled outputs in the model of Eq. 8, one can easily see that the resulting system is in the form of Eq. 5. Applying the method of moments to this system, utilizing the dimensionless variables of Eq. 11 and $\bar{u} = (c_0 - c_{0s})/(c_0 - c_s)$ and neglecting the moments of order four and higher, one can derive a system of the form of Eq. 25 with $\tilde{x} = [\tilde{x}_0 \ \tilde{x}_1 \ \tilde{x}_2 \ \tilde{x}_3 \ \tilde{y}]^T$ and

$$\tilde{f}(\tilde{x}) = \begin{bmatrix} -\tilde{x}_0 + (1-\tilde{x}_3)\,Da e^{-F/\tilde{y}^2} \\ -\tilde{x}_1 + \tilde{y}\tilde{x}_0 \\ -\tilde{x}_2 + \tilde{y}\tilde{x}_1 \\ -\tilde{x}_3 + \tilde{y}\tilde{x}_2 \\ \dfrac{1-\tilde{y}-(\alpha-\tilde{y})\tilde{y}\tilde{x}_2}{1-\tilde{x}_3} \end{bmatrix}, \quad \tilde{g}(\tilde{x}) = \begin{bmatrix} 0 \\ 0 \\ 0 \\ 0 \\ 1 \\ \dfrac{}{1-\tilde{x}_3} \end{bmatrix}$$

On the basis of this system, one can easily verify that assumptions 1, 2, and 3 of theorem 1 are satisfied. A direct application of the synthesis formula of Eq. 39 then yields the following nonlinear output feedback controllers

$$\frac{d\omega_0}{dt} = -\omega_0 + (1-\omega_3)\,Da e^{-F/\omega_4^2} + L_0\left[\tilde{h}(\tilde{x}) - \tilde{h}(\omega)\right]$$

$$\frac{d\omega_1}{dt} = -\omega_1 + \omega_4\omega_0 + L_1\left[\tilde{h}(\tilde{x}) - \tilde{h}(\omega)\right]$$

$$\frac{d\omega_2}{dt} = -\omega_2 + \omega_4\omega_1 + L_2\left[\tilde{h}(\tilde{x}) - \tilde{h}(\omega)\right]$$

$$\frac{d\omega_3}{dt} = -\omega_3 + \omega_4\omega_2 + L_3\left[\tilde{h}(\tilde{x}) - \tilde{h}(\omega)\right]$$

$$\frac{d\omega_4}{dt} = \frac{1-\omega_4-(\alpha-\omega_4)\omega_4\omega_2}{1-\omega_3} + L_4\left[\tilde{h}(\tilde{x}) - \tilde{h}(\omega)\right] + \frac{\left[\beta_2 L_{\tilde{g}} L_{\tilde{f}}\tilde{h}(\omega)\right]^{-1}\left\{\upsilon - \beta_0\tilde{h}(\omega) - \beta_1 L_{\tilde{f}}\tilde{h}(\omega) - \beta_2 L_{\tilde{f}}^2\tilde{h}(\omega)\right\}}{1-\omega_3}$$

$$\bar{u}(t) = \left[\beta_2 L_{\tilde{g}} L_{\tilde{f}}\tilde{h}(\omega)\right]^{-1} \times \left\{\upsilon - \beta_0\tilde{h}(\omega) - \beta_1 L_{\tilde{f}}\tilde{h}(\omega) - \beta_2 L_{\tilde{f}}^2\tilde{h}(\omega)\right\} \quad (42)$$

where υ is the set point, β_0, β_1, β_2, and $L = [L_0 \ L_1 \ L_2 \ L_3 \ L_4]^T$ are controller parameters and $\tilde{h}(\omega) = \omega_0$ or $\tilde{h}(\omega) = \omega_1$. The nonlinear controller of Eq. 42 was also combined with a PI controller [that is, the term $\upsilon - \beta_0\tilde{h}(\omega)$ was substituted by $\upsilon - \beta_0\tilde{h}(\tilde{x}) + (1/\tau_i')\xi$, where $\dot{\xi} = \upsilon - \tilde{h}(\tilde{x})$, $\xi(0) = 0$ and τ_i' is the integral time constant) to ensure offsetless tracking in the presence of constant uncertainty in process parameters. The practical implementation of the nonlinear controllers of Eq. 42 requires on-line measurements of the controlled outputs $\tilde{x}_0$ or $\tilde{x}_1$; in practice, such measurements can be obtained by using, for example, light scattering (Bohren and Huffman, 1983; Rawlings et al., 1993).

Table 3. Controller Parameters with $\tilde{x}_0$ as Controlled Output

	Without Disturbance/Delay	With Disturbance	With Delay
K_c	2.5	2.5	2.5
τ_i	0.5	0.5	1.0
L	$[1.0\ 0.0\ 0.0\ 0.0\ 1.0]^T$	$[1.0\ 0.0\ 0.0\ 0.0\ 1.0]^T$	$[1.0\ 0.0\ 0.0\ 0.0\ 1.0]^T$
β_0	1.0	1.0	1.0
β_1	2/3	2/3	2/3
β_2	1/9	1/9	1/9
τ_i'	20.0	20.0	20.0

Closed-loop simulations

Several simulation runs were performed to evaluate the performance and robustness properties of the nonlinear controllers of Eq. 42 and compare them with the ones of a PI controller. The values of the nonlinear controller parameters β_0, β_1, β_2 and L and the PI controller parameters K_c, τ_I, which were used in the simulations, are given in Tables 3 and 4 (K_c, τ_I were computed through extensive trial and error). In all the simulation runs, the initial condition

$$n(r,0) = 0.0, \quad c(0) = 990.0 \text{ kg/m}^3$$

was used for the process model of Eq. 8, and the finite difference method with 1,000 discretization points was used for its simulation. The initial conditions for the dynamic system included in the controller of Eq. 42 were set to be: $\omega_0 = 0.047$, $\omega_1 = 0.028$, $\omega_2 = 0.017$, $\omega_3 = 0.01$, and $\omega_4 = 0.5996$ (note that they do not correspond to the initial conditions used for the distributed parameter model in order to study the performance of the controller in the presence of significant initialization errors).

In the first set of simulation runs, $\tilde{x}_0$ was considered to be the controlled output. Initially, the set point tracking capability of the nonlinear controller was evaluated under nominal conditions for a 0.5 increase in the value of the set point ($\upsilon = 0.5$). Figure 5 shows the closed-loop output (top plot) and manipulated input (bottom plot) profiles obtained by using the nonlinear controller (solid lines) of Eq. 42. For the sake of comparison, the corresponding profiles under PI control are also included (dashed lines). Clearly, the nonlinear

Table 4. Controller Parameters with $\tilde{x}_1$ as Controlled Output

	Without Disturbance/Delay	With Disturbance	With Delay
K_c	2.5	2.5	2.0
τ_i	0.5	0.5	0.5
L	$[1.0\ 0.0\ 0.0\ 0.0\ 1.0]^T$	$[1.0\ 0.0\ 0.0\ 0.0\ 1.0]^T$	$[1.0\ 0.0\ 0.0\ 0.0\ 1.0]^T$
β_0	1.0	1.0	1.0
β_1	2.0	2.0	2.0
β_2	1.0	1.0	1.0
τ_i'	20.0	20.0	20.0

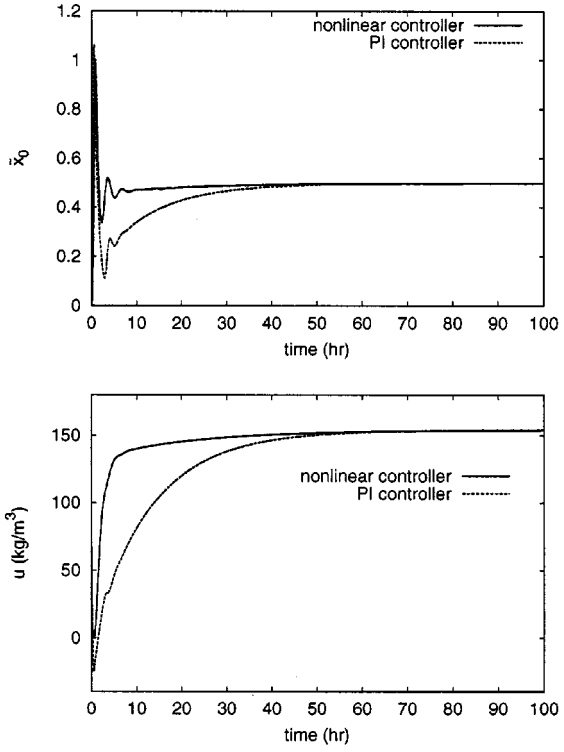

Figure 5. Closed-loop output (top) and manipulated input (bottom) under nonlinear and PI control for a 0.5 increase in the set point.

$\tilde{x}_0$ is the controlled output.

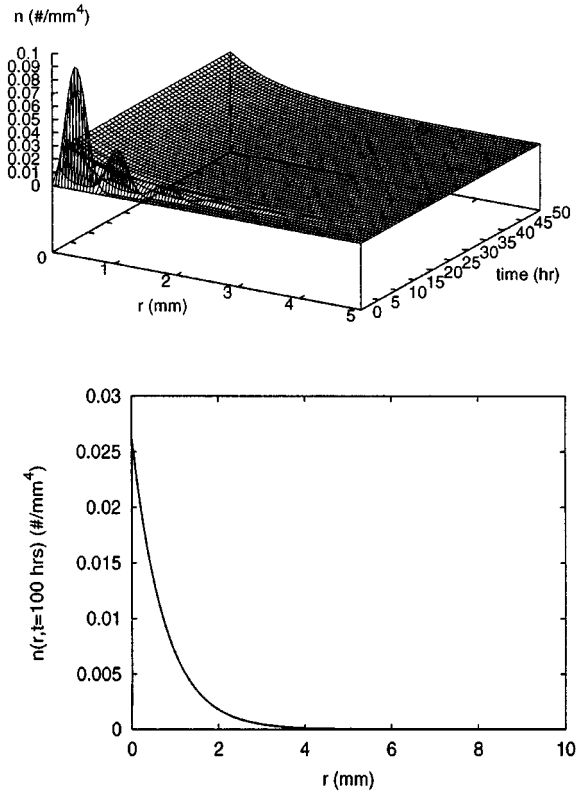

Figure 6. Evolution of crystal-size distribution (top) and final steady-state crystal-size distribution (bottom) under nonlinear control.

$\tilde{x}_0$ is the controlled output.

controller drives the controlled output to its new set point value in a significantly shorter time than the one required by the PI controller (note that both controlled outputs exhibit the same overshoot). For the same simulation run, the evolution of the closed-loop profile and the final steady-state profile of the crystal-size distribution are shown in Figure 6. An exponentially-decaying crystal-size distribution is obtained at the steady state. Next, the robustness properties of the nonlinear controller in the presence of parametric uncertainties, unmodeled dynamics, and measurement sensor dead-time were investigated for a 0.5 increase in the value of the set point. Figures 7 and 8 show the closed-loop output (top plot) and manipulated input (bottom plot) profiles under the nonlinear controller (solid lines) in the presence of 5% error in both F and τ, and in the presence of fast actuator dynamics. To account for the actuator dynamics, the process model of Eq. 6 was augmented with the dynamical system $\epsilon_z \dot{z}_1 = -z_1 + z_2$, $\epsilon_z \dot{z}_2 = -z_2 + u$, where $z_1, z_2 \in \mathbb{R}$ are the actuator states, z_1 is the actuator output and ϵ_z is a small parameter characterizing how fast are the actuator dynamics. The corresponding output and input profiles under PI control are also included (dashed lines). In the case of parametric uncertainties, the nonlinear controller exhibits very good robustness properties, driving quickly the output to its new set point. In the case of unmodeled actuator dynamics, the nonlinear controller was also found to be more robust since the maximum ϵ_z, for which a stable closed-loop system was obtained, under nonlinear control is $\epsilon_z = 0.04$, while under proportional integral control $\epsilon_z = 0.02$. Finally, a 10.0 min delay in the measurement sensor was considered and the nonlinear controller of Eq. 42 was redesigned within a Smith-Predictor framework, according to the results in Antoniades and Christofides (1999) (details are omitted for brevity) to account for the presence of the delay. Figure 9 shows the profiles of the controlled outputs (top plot) and manipulated inputs (bottom plot) under nonlinear (solid lines) and PI (dashed lines) control for a 0.5 increase in the value of the set point. Clearly, the presence of the measurement delay deteriorates significantly the output response under PI control (note the oscillations of the controlled output), while it affects very little the output response under nonlinear control.

In the second set of simulation runs, $\tilde{x}_1$ was considered to be the controlled output. Initially, the performance of the nonlinear controller for a 0.5 increase in the value of the set point was tested under nominal conditions. Figure 10 shows the closed-loop output (top plot) and manipulated input (bottom plot) profiles under nonlinear (solid lines) and PI (dashed lines) control. Again, the nonlinear controller drives the output to its new set point much faster than the PI controller. The closed-loop profile of the evolution of the crystal-size distribution is plotted in Figure 11 (top plot), along with the final steady-state profile of the crystal-size distribution (middle plot) and the evolution of the mean crystal size (bottom plot). The stabilization of the crystal-size distribution is

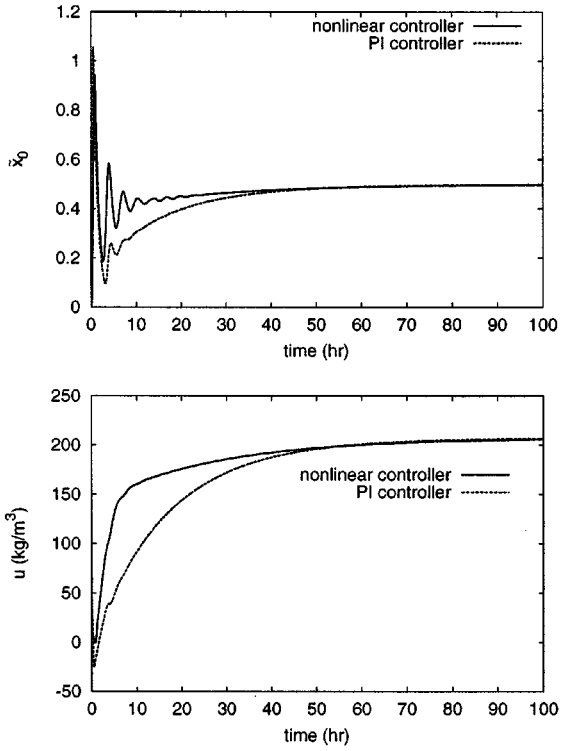

Figure 7. Closed-loop output (top) and manipulated input (bottom) under nonlinear and PI control for a 0.5 increase in the set point in the presence of a 5% modeling error in both F and τ.

$\tilde{x}_0$ is the controlled output.

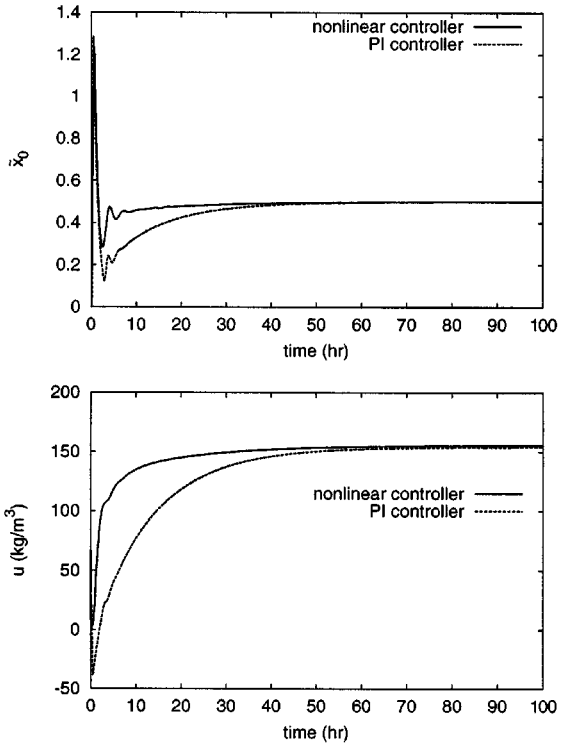

Figure 8. Closed-loop output (top) and manipulated input (bottom) under nonlinear and PI control for a 0.5 increase in the set point in the presence of unmodeled actuator dynamics.

$\tilde{x}_0$ is the controlled output.

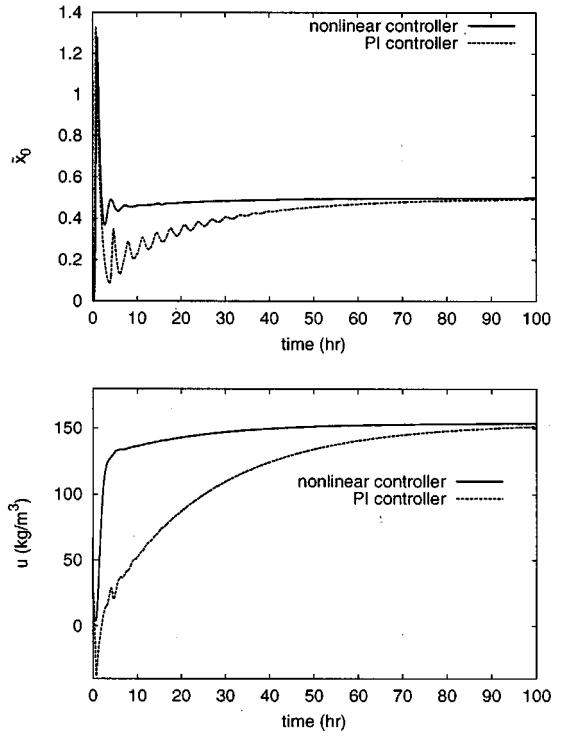

Figure 9. Closed-loop output (top) and manipulated input (bottom) under nonlinear and PI control for a 0.5 increase in the set point in the presence of a 10.0 min delay in the output measurements.

$\tilde{x}_0$ is the controlled output.

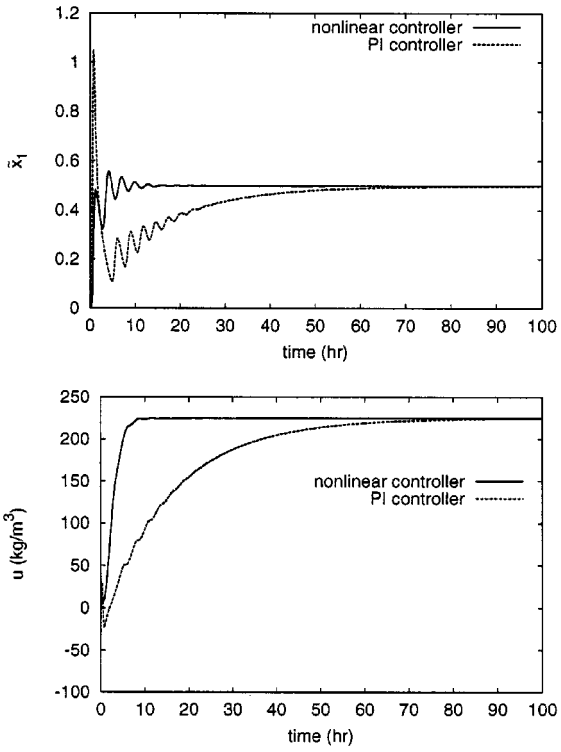

Figure 10. Closed-loop output (top) and manipulated input (bottom) under nonlinear and PI control for a 0.5 increase in the set point.

$\tilde{x}_1$ is the controlled output.

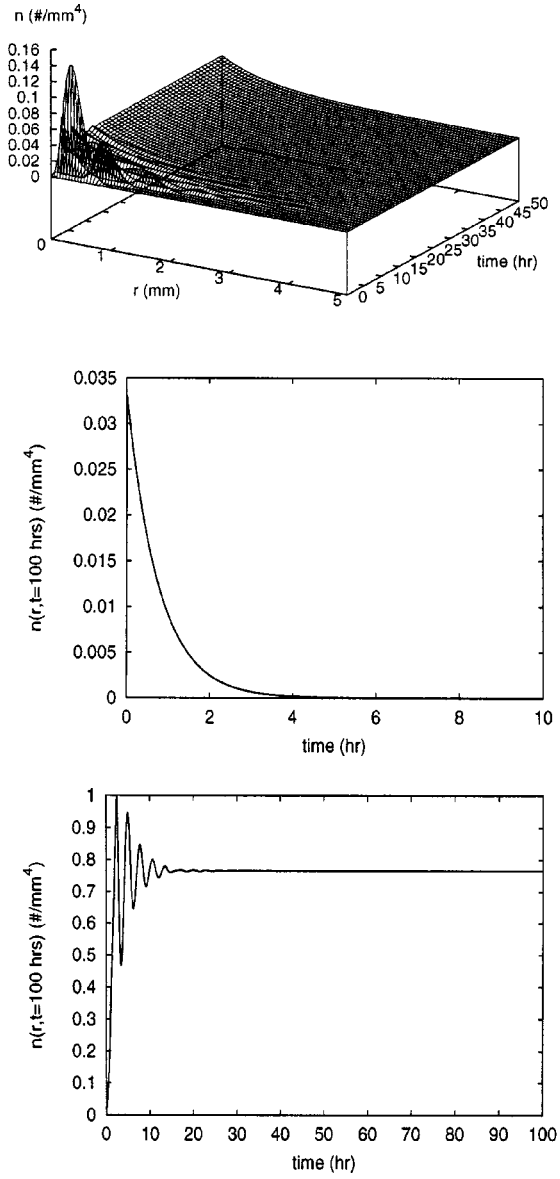

Figure 11. Profile of evolution of crystal-size distribution (top), final steady-state crystal-size distribution (middle), and evolution of mean crystal size (bottom) under nonlinear control.

$\tilde{x}_1$ is the controlled output.

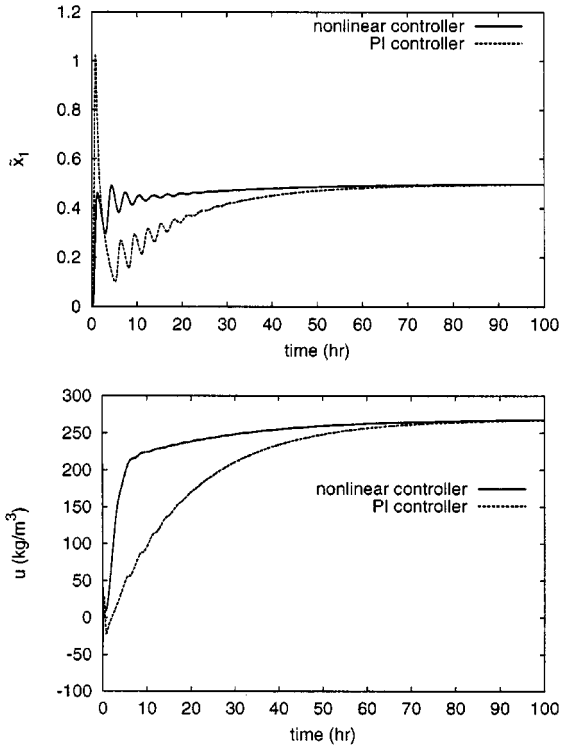

Figure 12. Closed-loop output (top) and manipulated input (bottom) under nonlinear and PI control for a 0.5 increase in the set point in the presence of a 5% modeling error in both *F* and τ.

$\tilde{x}_1$ is the controlled output.

quickly achieved and an exponentially-decaying crystal-size distribution is obtained at steady state. Moreover, the final steady-state mean crystal size $\tilde{x}_1/\tilde{x}_0 = 0.77$ is about 28% higher than the mean crystal size of the open-loop unstable steady-state $\tilde{x}_1/\tilde{x}_0 = 0.60$, establishing that control of $\tilde{x}_1$ allows regulating the mean crystal size at a desired value. The robustness properties of the nonlinear controller in the presence of parametric uncertainties, unmodeled dynamics, and measurement sensor dead-time were also investigated. Initially, a 5% error in both F and τ, and unmodeled actuator dynamics, as described above, were separately considered.

Figures 12 and 13 show the resulting closed-loop output (top plot) and manipulated input (bottom plot) profiles under nonlinear (solid lines) and PI (dashed lines) control. It is clear that the nonlinear controller possesses very good robustness properties with respect to parametric uncertainties, attenuating their effect on the output. Also, the nonlinear controller was found to be more robust with respect to unmodeled dynamics $\epsilon_z = 0.02$, compared to the proportional integral controller $\epsilon_z = 0.01$. Finally, a delay of 10.0 min in the output measurement was considered (again, the nonlinear controller of Eq. 42 was redesigned within a Smith-Predictor framework to account for the measurement delay). Figure 14 presents the output (top) and manipulated input (bottom) profiles under nonlinear (solid lines) and PI (dashed lines) control. Again, the superior performance of the nonlinear controller is evident.

Remark 19. We note that the fifth-order model of Eq. 14, which was used for the design of the nonlinear output feedback controllers of Eq. 42, was obtained by using the method of moments and no improvement of its accuracy was pursued by using approximate inertial manifolds. The reason is that the closed-loop performance and robustness properties of the controllers of Eq. 42 are clearly excellent (see the closed-loop output profiles in Figures 5 and 10, respectively), thereby leaving no room for further improvement of the performance of the controller by using approximate inertial manifolds.

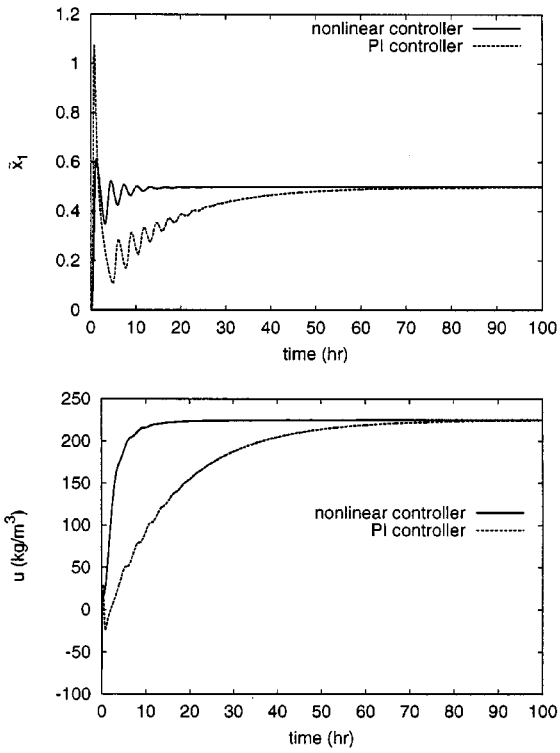

Figure 13. Closed-loop output (top) and manipulated input (bottom) under nonlinear and PI control for a 0.5 increase in the set point in the presence of unmodeled actuator dynamics.

$\tilde{x}_1$ is the controlled output.

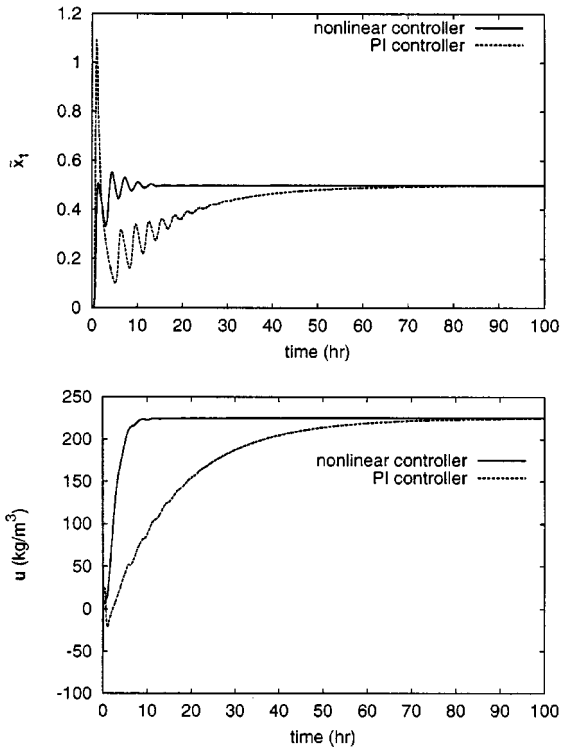

Figure 14. Closed-loop output (top) and manipulated input (bottom) under nonlinear and PI control for a 0.5 increase in the set point in the presence of a 10.0 min delay in the output measurements.

$\tilde{x}_1$ is the controlled output.

Conclusions

In this work, we considered spatially-homogeneous particulate processes modeled by a class of nonlinear partial integro-differential equation systems and developed a rigorous and general method for the synthesis of practically-implementable nonlinear output feedback controllers. The controllers enforce stability and attain a particle-size distribution (PSD) with desired characteristics in the closed-loop system. Initially, a model reduction procedure based on a combination of the method of weighted residuals and the concept of approximate inertial manifold was presented for the construction of low-order ODE systems that accurately reproduce the dynamics of the particulate process. These ODE systems were then used for the synthesis of nonlinear low-order output feedback controllers that enforce exponential stability in the closed-loop system and achieve a desired PSD. The performance and robustness properties of the proposed control method were successfully tested through simulations on a continuous crystallizer which exhibits open-loop unstable (oscillatory) behavior and were shown to be superior to the ones of a proportional integral controller.

Acknowledgment

Financial support from a National Science Foundation CAREER award, CTS 9733509, is gratefully acknowledged.

Literature Cited

Antoniades, C., and P. D. Christofides, "Feedback Control of Nonlinear Differential Difference Equation Systems," *Chem. Eng. Sci.*, in press (1999).

Bohren, C. F., and D. R. Huffman, *Absorption and Scattering of Light by Small Particles*, Wiley, New York (1983).

Christofides, P. D., and P. Daoutidis, "Feedback Control of Hyperbolic PDE Systems," *AIChE J.*, **42**, 3063 (1996a).

Christofides, P. D., and P. Daoutidis, "Nonlinear Control of Diffusion-Convection-Reaction Processes," *Comp. Chem. Eng.*, **20**(s), 1071 (1996b).

Dimitratos, J., G. Elicabe, and C. Georgakis, "Control of Emulsion Polymerization Reactors," *AIChE J.*, **40**, 1993 (1994).

Eaton, J. W., and J. B. Rawlings, "Feedback Control of Chemical Processes Using On-Line Optimization Techniques," *Comp. Chem. Eng.*, **14**, 469 (1990).

Foias, C., and R. Témam, "Algebraic Approximation of Attractors: The Finite Dimensional Case," *Physica D*, **32** 163 (1988).

Friedlander, S. K., *Smoke, Dust, and Haze: Fundamentals of Aerosol Behavior*, Wiley, New York (1977).

Fukunaga, K., *Introduction to Statistical Pattern Recognition*, Academic Press, New York (1990).

Gelbard, F., and J. H. Seinfeld, "Numerical Solution of the Dynamic Equation for Particulate Processes," *J. Comp. Phys.*, **28**, 357 (1978).

Gelbard, F., Y. Tambour, and J. H. Seinfield, "Sectional Representation of Simulating Aerosol Dynamics," *J. Coll. Int. Sci.*, **68**, 363 (1980).

Hill, P. J., and K. M. Ng, "New Discretization Procedure for the Agglomeration Equation," *AIChE J.*, **42**, 727 (1996).

Holmes, P., J. L. Lumley, and G. Berkooz, *Turbulence, Coherent*

Structures, Dynamical Systems and Symmetry, Cambridge University Press, New York (1996).
Hounslow, M. J., "A Discretized Population Balance for Continuous Systems at Steady-State," *AIChE J.*, **36**, 106 (1990).
Hulburt, H. M., and S. Katz, "Some Problems in Particle Technology: A Statistical Mechanical Formulation," *Chem. Eng. Sci.*, **19**, 555 (1964).
Isidori, A., *Nonlinear Control Systems: An Introduction*, 2nd ed., Springer-Verlag, Berlin-Heidelberg (1989).
Jerauld, G. R., Y. Vasatis, and M. F. Doherty, "Simple Conditions for the Appearance of Sustained Oscillations in Continuous Crystallizers," *Chem. Eng. Sci.*, **38**, 1675 (1983).
Khalil, H. K., *Nonlinear Systems*, Macmillan, New York (1992).
Kumar, S., and D. Ramkrishna, "On the Solution of Population Balance Equations by Discretization—I. A Fixed Pivot Technique," *Chem. Eng. Sci.*, **51**, 1311 (1996a).
Kumar, S., and D. Ramkrishna, "On the Solution of Population Balance Equations by Discretization—II. A Moving Pivot Technique," *Chem. Eng. Sci.*, **51**, 1333 (1996b).
Kurtz, M. J., G.-Y. Zhu, A. Zamamiri, M. A. Henson, and M. A. Hjortso, "Control of Oscillating Microbial Cultures Described by Population Balance Models," *Ind. Eng. Chem. Res.*, **37**, 4059 (1998).
Landgrebe, J. D., and S. E. Pratsinis, "A Discrete Sectional Model for Particulate Production by Gas Phase Chemical Reaction and Aerosol Coagulation in the Free Molecular Regime," *J. Coll. Inter. Sci.*, **139**, 63 (1990).
Lei, S. J., R. Shinnar, and S. Katz, "The Stability and Dynamic Behavior of a Continuous Crystallizer with a Fines Trap," *AIChE J.*, **17**, 1459 (1971).
Pratsinis, S. E., "Simultaneous Nucleation, Condensation, and Coagulation in Aerosol Reactors," *J. Coll. Int. Sci.*, **124**, 416 (1988).
Ramkrishna, D., "The Status of Population Balances," *Rev. Chem. Eng.*, **3** 49 (1985).
Randolph, A. D., L. Chen, and A. Tavana, "Feedback Control of CSD in a KCl Crystallizer with a Fines Dissolver," *AIChE J.*, **33**, 583 (1987).
Randolph, A. D., and M. A. Larson, *Theory of Particulate Processes*, Academic Press, 2nd ed., San Diego (1988).
Rawlings, J. B., S. M. Miller and W. R. Witkowski, "Model Identification and Control of Solution Crystallization Processes," *I & EC Res.*, **32**, 1275 (1993).
Rawlings, J. B., and W. H. Ray, "Emulsion Polymerization Reactor Stability: Simplified Model Analysis," *AIChE J.*, **33**, 1663 (1987a).
Rawlings, J. B., and W. H. Ray, "Stability of Continuous Emulsion Polymerization Reactors: a Detailed Model Analysis," *Chem. Eng. Sci.*, **42**, 2767 (1987b).
Rohani, S., and J. R. Bourne, "Self-Tuning Control of Crystal Size Distribution in a Cooling Batch Crystallizer," *Chem. Eng. Sci.*, **12**, 3457 (1990).
Semino, D., and W. H. Ray, "Control of Systems Described by Population Balance Equations—I. Controllability Analysis," *Chem. Eng. Sci.*, **50**, 1805 (1995a).
Semino, D., and W. H. Ray, "Control of Systems Described by Population Balance Equations—II. Emulsion Polymerization with Constrained Control Action," *Chem. Eng. Sci.*, **50**, 1825 (1995b).
Shvartsman, S. Y., and I. G. Kevrekidis, "Nonlinear Model Reduction for Control of Distributed Parameter Systems: A Computer Assisted Study," *AIChE J.*, **44**, 1579 (1998).
Temam, R., *Infinite-Dimensional Dynamical Systems in Mechanics and Physics*, Springer-Verlag, New York (1988).
Williams, M. M. R., and S. K. Loyalka, *Aerosol Science: Theory & Practice*, Pergamon Press, Oxford, U.K. (1991).

Appendix

Proof of proposition 1

To simplify the notation of the proof, we assume that the growth rate $G(x, r)$ is independent of r. Furthermore, since the nonlinear terms $w(n, x, r)$, $a(n, r, x)$ are smooth functions of their arguments, they can be exactly expanded in an infinite series as follows

$$w(n,x,r)=\sum_{k=1}^{\infty} b_k(x,a_k,t)\phi_k(r)$$

$$a(n,r,x)=\sum_{k=1}^{\infty} c_k(x,a_k,t)\phi_k(r) \qquad \text{(A1)}$$

where $b_k(x, a_k, t)$, $c_k(x, a_k, t)$ are coefficients and $\phi_k(r)$, $k = 1, \ldots, \infty$ is the complete set of basis functions used to expand $n(r, t)$ in Eq. 17. Using that, $G(x, r)$ is independent of r and the expansions of Eq. A1, the infinite dimensional system of Eq. 19, can be written as

$$\int_0^{r_{\max}}\psi_\nu(r)\sum_{k=1}^{\infty}\phi_k(r)\frac{\partial a_k(t)}{\partial t}dr$$
$$=-G(x)\sum_{k=1}^{\infty}a_k(t)\int_0^{r_{\max}}\psi_\nu(r)\frac{\partial\phi_k(r)}{\partial r}dr$$
$$+\int_0^{r_{\max}}\psi_\nu(r)\sum_{k=1}^{\infty}b_k(x,a_k,t)\phi_k(r)dr, \quad \nu=1,\ldots,\infty$$
$$\dot{x}=f(x)+A\int_0^{r_{\max}}\sum_{k=1}^{\infty}c_k(x,a_k,t)\phi_k(r)dr \qquad \text{(A2)}$$

while the truncated system of Eq. 20 takes the form

$$\int_0^{r_{\max}}\psi_\nu(r)\sum_{k=1}^{N}\phi_k(r)\frac{\partial a_{kN}(t)}{\partial t}dr$$
$$=-G(x_N)\sum_{k=1}^{N}a_{kN}(t)\int_0^{r_{\max}}\psi_\nu(r)\frac{\partial\phi_k(r)}{\partial r}dr$$
$$+\int_0^{r_{\max}}\psi_\nu(r)\sum_{k=1}^{N}b_k(x_N,a_{kN},t)\phi_k(r)dr, \quad \nu=1,\ldots,N$$
$$\dot{x}_N=f(x_N)+A\int_0^{r_{\max}}\sum_{k=1}^{N}c_k(x_N,a_{kN},t)\phi_k(r)dr \qquad \text{(A3)}$$

Defining the error variables $e_n = n(r, t) - n_N(r, t) = \sum_{k=1}^{\infty} a_k(t)\phi_k(r) - \sum_{k=1}^{N} a_{kN}(t)\phi_k(r)$ and $e_x = x(t) - x_N(t)$ and computing the difference between Eq. A2 and Eq. A3, we get

$$\int_0^{r_{\max}}\psi_\nu(r)\frac{\partial e_n}{\partial t}dr$$
$$=-G(x)\int_0^{r_{\max}}\psi_\nu(r)\frac{\partial n}{\partial r}dr+G(x_N)\int_0^{r_{\max}}\psi_\nu(r)\frac{\partial n_N}{\partial r}dr$$
$$+\int_0^{r_{\max}}\psi_\nu(r)\sum_{k=1}^{\infty}b_k(x,a_k,t)\phi_k(r)dr$$
$$-\int_0^{r_{\max}}\psi_\nu(r)\sum_{k=1}^{N}b_k(x_N,a_{kN},t)\phi_k(r)dr$$
$$\dot{e}_x=f(x)-f(x_N)+A\int_0^{r_{\max}}\sum_{k=1}^{\infty}c_k(x,a_k,t)\phi_k(r)dr$$
$$-A\int_0^{r_{\max}}\sum_{k=1}^{N}c_k(x_N,a_{kN},t)\phi_k(r)dr \qquad \text{(A4)}$$

The above error system is locally exponentially stable (this follows from the assumption that the system of Eq. 20 is locally exponentially stable for any N), and, thus, applying standard results from perturbation theory (Khalil, 1992, Theorem 8.2), we have that there exists an N sufficiently large so that the following results hold for $e_n(r,t)$, $e_x(t)$ for all $t \geq 0$

$$e_n(r,t) = O[\epsilon(N)]$$
$$e_x(t) = O[\epsilon(N)] \tag{A5}$$

From the above result, the estimates of Eq. 21 follow directly.

Proof of proposition 2

To prove that local exponential stability of the system of Eq. 32 ensures local exponential stability of the system of Eq. 20, we need to show that the off manifold transients decay exponentially. To this end, we define $e_m = a_{fN} - \tilde{\Sigma}_{l+1}(\tilde{x}) = a_{fN} - \tilde{a}_{fN}$ and compute $\dot{e}_m$

$$\dot{e}_m = \tilde{A}a_{fN} + \tilde{f}_q(a_{fN}, \tilde{x}) - \dot{\tilde{a}}_{fN} \tag{A6}$$

From the definition of the approximate inertial manifold $\dot{\tilde{a}}_{fN} \equiv 0 = \tilde{A}\tilde{a}_{fN} + \tilde{f}_q(\tilde{a}_{fN}, \tilde{x})$, and, thus, the system of Eq. A6 can be written as

$$\begin{aligned}\dot{e}_m &= \tilde{A}a_{fN} + \tilde{f}_q(a_{fN}, \tilde{x}) - \tilde{A}\tilde{a}_{fN} - \tilde{f}_q(\tilde{a}_{fN}, \tilde{x}) \\ &= \tilde{A}e_m + \tilde{f}_q(a_{fN}, \tilde{x}) - \tilde{f}_q(\tilde{a}_{fN}, \tilde{x})\end{aligned} \tag{A7}$$

Since $\tilde{A}$ is Hurwitz, the terms $\tilde{f}_q(a_{fN}, \tilde{x})$, $\tilde{f}_q(\tilde{a}_{fN}, \tilde{x})$ do not include linear terms and the system of Eq. 32 is locally exponentially stable, one can show that the linearization of the system of Eq. 26 is exponentially stable, and, thus, the nonlinear system is locally exponentially stable.

To establish the closeness of solutions result, we exploit the fact that the local exponential stability implies (Khalil, 1992) $a_{kN}(t) = \tilde{a}_{kN}(t) + \bar{\epsilon}(\tilde{l})$, and also that $\Sigma(\tilde{x}) = \tilde{\Sigma}_{l+1}(\tilde{x}) + \bar{\epsilon}(\tilde{l})$, as $t \to \infty$. Computing the $\lim_{t\to\infty}\|n_N - \bar{n}_N\|_2$, using the above estimates, it can be shown that $\lim_{t\to\infty}\|n_N - \bar{n}_N\|_2 = O[\bar{\epsilon}(\tilde{l})]$.

Proof of theorem 1

Under the controller of Eq. 39, the closed-loop system takes the form

$$\frac{d\omega}{dt} = \tilde{f}(\omega) + L\left[y - \tilde{h}(\omega)\right] + \tilde{g}(\omega)$$
$$\times\left\{\left[\beta_{1r_1} \cdots \beta_{mr_m}\right]C(\omega)\right\}^{-1}\left\{\upsilon - \sum_{i=1}^{m}\sum_{k=0}^{r_i}\beta_{ik}L_{\tilde{f}}^{k}\tilde{h}_i(\omega)\right\}$$

$$\frac{\partial n}{\partial t} = -\frac{\partial[G(x,r)n]}{\partial r} + w(n,x,r)$$

$$\dot{x} = f(x) + A\int_0^{r_{\max}} a(n,r,x)\,dr + g(x)$$
$$\times\left\{\left[\beta_{1r_1} \cdots \beta_{mr_m}\right]C(\omega)\right\}^{-1}\left\{\upsilon - \sum_{i=1}^{m}\sum_{k=0}^{r_i}\beta_{ik}L_{\tilde{f}}^{k}\tilde{h}_i(\omega)\right\} \tag{A8}$$

Applying the method of weighted residuals to the above system, we obtain the following approximate ODE system

$$\frac{d\omega}{dt} = \tilde{f}(\omega) + L\left[y - \tilde{h}(\omega)\right] + \tilde{g}(\omega)$$
$$\times\left\{\left[\beta_{1r_1} \cdots \beta_{mr_m}\right]C(\omega)\right\}^{-1}\left\{\upsilon - \sum_{i=1}^{m}\sum_{k=0}^{r_i}\beta_{ik}L_{\tilde{f}}^{k}\tilde{h}_i(\omega)\right\}$$

$$\int_0^{r_{\max}}\psi_\nu(r)\sum_{k=1}^{N}\phi_k(r)\frac{\partial a_{kN}(t)}{\partial t}dr$$
$$= -\sum_{k=1}^{N}a_{kN}(t)\int_0^{r_{\max}}\psi_\nu(r)\frac{\partial[G(x_N,r)\phi_k(r)]}{\partial r}dr$$
$$+\int_0^{r_{\max}}\psi_\nu(r)w\left[\sum_{k=1}^{N}a_{kN}(t)\phi_k(r), x_N, r\right]dr, \quad \nu = 1, \ldots, N$$

$$\dot{x}_N = f(x_N) + A\int_0^{r_{\max}} a\left[\sum_{k=1}^{N}a_{kN}(t)\phi_k(r), r, x_N\right]dr + g(x_N)$$
$$\times\left\{\left[\beta_{1r_1} \cdots \beta_{mr_m}\right]C(\omega)\right\}^{-1}\left\{\upsilon - \sum_{i=1}^{m}\sum_{k=0}^{r_i}\beta_{ik}L_{\tilde{f}}^{k}\tilde{h}_i(\omega)\right\} \tag{A9}$$

Using the vector notation $a_N = [a_{1N} \cdots a_{NN}]^T$, the above system can be written as

$$\frac{d\omega}{dt} = \tilde{f}(\omega) + L\left[y - \tilde{h}(\omega)\right] + \tilde{g}(\omega)$$
$$\times\left\{\left[\beta_{1r_1} \cdots \beta_{mr_m}\right]C(\omega)\right\}^{-1}\left\{\upsilon - \sum_{i=1}^{m}\sum_{k=0}^{r_i}\beta_{ik}L_{\tilde{f}}^{k}\tilde{h}_i(\omega)\right\}$$

$$\dot{a}_N = \tilde{f}(a_N, x_N)$$

$$\dot{x}_N = f(x_N) + A\int_0^{r_{\max}} a\left[\sum_{k=1}^{N}a_{kN}(t)\phi_k(r), x_N, r\right]dr + g(x_N)$$
$$\times\left\{\left[\beta_{1r_1} \cdots \beta_{mr_m}\right]C(\omega)\right\}^{-1}\left\{\upsilon - \sum_{i=1}^{m}\sum_{k=0}^{r_i}\beta_{ik}L_{\tilde{f}}^{k}\tilde{h}_i(\omega)\right\} \tag{A10}$$

where the explicit form of the nonlinear function $\tilde{f}(a_N, x_N)$ is omitted for brevity. Exploiting the orthogonality of the basis functions $\phi_k(r)$ and using the expression for n_N of Eq. 24,

we can write the system of Eq. A10 as

$$\frac{d\omega}{dt} = \tilde{f}(\omega) + L\left[y - \tilde{h}(\omega)\right] + \tilde{g}(\omega)$$
$$\times\left\{\left[\beta_{1r_1} \cdots \beta_{mr_m}\right]C(\omega)\right\}^{-1}\left\{\upsilon - \sum_{i=1}^{m}\sum_{k=0}^{r_i}\beta_{ik}L_{\tilde{f}}^{k}\tilde{h}_i(\omega)\right\}$$
$$\dot{a}_{sN} = \bar{f}_p(a_{sN}, a_{fN}, x_N)$$
$$\dot{a}_{fN} = \bar{f}_q(a_{sN}, a_{fN}, x_N)$$
$$\dot{x}_N = f(x_N) + A\int_0^{r_{\max}} a(n_p + n_q, x_N, r)\,dr + g(x_N)$$
$$\times\left\{\left[\beta_{1r_1} \cdots \beta_{mr_m}\right]C(\omega)\right\}^{-1}\left\{\upsilon - \sum_{i=1}^{m}\sum_{k=0}^{r_i}\beta_{ik}L_{\tilde{f}}^{k}\tilde{h}_i(\omega)\right\} \quad \text{(A11)}$$

where $\bar{f} = [\bar{f}_p^T\ \bar{f}_q^T]^T$, $a_{sN} = [a_{1N} \cdots a_{pN}]^T$, and $a_{fN} = [a_{(p+1)N} \cdots a_{NN}]^T$. Defining the observer error vector $e_o = \omega - \tilde{x}$, using the assumption $C_L = (1/\mu)\bar{A}$, where $\bar{A}$ is a Hurwitz matrix, and multiplying the $\dot{e}_o$-subsystem by μ, the system of Eq. A11 can be written as

$$\mu\frac{de_o}{dt} = \bar{A}e_o + \mu\hat{f}(\omega, \tilde{x}, \upsilon)$$
$$\dot{a}_{sN} = \bar{f}_p(a_{sN}, a_{fN}, x_N)$$
$$\dot{a}_{fN} = \bar{f}_q(a_{sN}, a_{fN}, x_N)$$
$$\dot{x}_N = f(x_N) + A\int_0^{r_{\max}} a(n_p + n_q, x_N, r)\,dr + g(x_N)$$
$$\times\left\{\left[\beta_{1r_1} \cdots \beta_{mr_m}\right]C(\omega)\right\}^{-1}\left\{\upsilon - \sum_{i=1}^{m}\sum_{k=0}^{r_i}\beta_{ik}L_{\tilde{f}}^{k}\tilde{h}_i(\omega)\right\} \quad \text{(A12)}$$

where $\hat{f}(\omega, \tilde{x}, \upsilon)$ is a nonlinear vector function. The above system is in singularly perturbed form [see Khalil (1992) for details] and possesses an exponentially stable fast subsystem: $de_o/d\tau = \bar{A}e_o$, where $\tau = t/\mu$, and a slow subsystem that has the form

$$\dot{a}_{sN} = \bar{f}_p(a_{sN}, a_{fN}, x_N)$$
$$\dot{a}_{fN} = \bar{f}_q(a_{sN}, a_{fN}, x_N)$$
$$\dot{x}_N = f(x_N) + A\int_0^{r_{\max}} a(n_p + n_q, x_N, r)\,dr + g(x_N)$$
$$\times\left\{\left[\beta_{1r_1} \cdots \beta_{mr_m}\right]C(\tilde{x})\right\}^{-1}\left\{\upsilon - \sum_{i=1}^{m}\sum_{k=0}^{r_i}\beta_{ik}L_{\tilde{f}}^{k}\tilde{h}_i(\tilde{x})\right\} \quad \text{(A13)}$$

Setting $a_{fN} = \tilde{\Sigma}_{\bar{l}+1}(a_{sN}, x_N)$ (model reduction based on the concept of approximate inertial manifold) and using the notation of the subsection on inertial manifold, we finally obtain

$$\dot{\tilde{x}} = \tilde{f}(\tilde{x}) + \tilde{g}(\tilde{x})$$
$$\times\left\{\left[\beta_{1r_1} \cdots \beta_{mr_m}\right]C(\tilde{x})\right\}^{-1}\left\{\upsilon - \sum_{i=1}^{m}\sum_{k=0}^{r_i}\beta_{ik}L_{\tilde{f}}^{k}\tilde{h}_i(\tilde{x})\right\}$$
$$y_{s_i} = \tilde{h}_i(\tilde{x}), \quad i = 1, \ldots, m \quad \text{(A14)}$$

Using assumptions 2 and 3 of the theorem, one can show that the above system is locally exponentially stable and $\lim_{t\to\infty}|y_{s_i} - \upsilon_i| = 0$. From the assumption that $\bar{l}$ is sufficiently large and proposition 2, we have that the system of Eqs. A13 and A14 possess the same stability properties, and, thus, the slow subsystem of Eq. A13 is also locally exponentially stable. The local exponential stability of the fast and slow subsystems implies (Khalil, 1992) that there exists a μ^* such that if $\mu \in (0, \mu^*]$, then the closed-loop system of Eq. A11 is locally exponentially stable. From the closeness of solutions results of propositions 1 and 2, the asymptotic output tracking result $\lim_{t\to\infty}|y_i - \upsilon_i| = O[\hat{\epsilon}(N + \bar{l})]$ then follows.

Manuscript received Sept. 10, 1998, and revision received Mar. 22, 1999.